Thermochromic Properties of VO_2 + ZrO_2 Based Bi- and Triple- Layer Thin Films for Optical Applications

A thesis Submitted to the College of

Graduate and Postdoctoral Studies

In Partial Fulfillment of the Requirements

For the Degree of Master of Science

In the Department of Mechanical Engineering

University of Saskatchewan

Saskatoon Saskatchewan Canada

By

Justin Tricsli

© Copyright Justin Bruce Tricsli, August, 2024. All rights reserved.
Unless otherwise noted, copyright of the material in this thesis belongs to the author

PERMISSION TO USE

In presenting this thesis/dissertation in partial fulfillment of the requirements for a Postgraduate degree from the University of Saskatchewan, I agree that the Libraries of this University may make it freely available for inspection. I further agree that permission for copying of this thesis/dissertation in any manner, in whole or in part, for scholarly purposes may be granted by the professor or professors who supervised my thesis/dissertation work or, in their absence, by the Head of the Department or the Dean of the College in which my thesis work was done. It is understood that any copying or publication or use of this thesis/dissertation or parts thereof for financial gain shall not be allowed without my written permission. It is also understood that due recognition shall be given to me and to the University of Saskatchewan in any scholarly use which may be made of any material in my thesis/dissertation.

Requests for permission to copy or to make other uses of materials in this thesis/dissertation in whole or part should be addressed to:

Head of the Mechanical Engineering Department
57 Campus Drive
University of Saskatchewan
Saskatoon, Saskatchewan S7N 5A9 Canada

OR

Dean
College of Graduate and Postdoctoral Studies
University of Saskatchewan
116 Thorvaldson Building, 110 Science Place
Saskatoon, Saskatchewan S7N 5C9 Canada

ABSTRACT

Vanadium dioxide (VO_2) films have shown usefulness as a part of optoelectrical devices due to rapid reversible phase transition which sees large changes in both optical and electric properties. This transition sees insulating monoclinic structure films with high optical transmittance and electrical resistivity change at 69 °C to metallic rutile structure which has low optical transmittance and electrical resistivity. Potential utilizations of VO_2 films include smart windows, optical and electrical switching, and smart radiators for small satellites. Application designs regularly require additional oxide layers. Zirconium dioxide shows promise as an additional oxide layer due to high robustness, and compatible optical/structural properties. Due to vanadium having a high number of oxidative states, VO_2 films are sensitive to oxidation and are difficult to manufacture at a high quality.

In this current study, three different layered designs that include VO_2 and ZrO_2 layers were synthesized by reactive magnetron sputtering on Si and sapphire substrates. Layer designs include two bi-layers, which have ZrO_2 as a base layer with VO_2 deposited on top (ZrO_2/VO_2), and the reverse with ZrO_2 deposited on top of a VO_2 layer (VO_2/ZrO_2). Two triple-layer designs with a VO_2 layer between ZrO_2 layers ($ZrO_2/VO_2/ZrO_2$) were deposited with different top layer deposition temperatures of 500 °C and 650 °C. The effect of these different layer designs on the structure of these films showed oxidization of VO_2 films when ZrO_2 is deposited as a top layer in Raman spectroscopy and SEM testing. These films showed incomplete transitions upon heating but still may be useable in applications that do not require a complete transition such as smart windows. ZrO_2/VO_2 samples showed no oxidization and had sharp, complete transitions in optical testing. The effect of this structural change was found to outweigh changes in roughness found in these samples. These results suggest that designs for switching that require full transition should use VO_2 deposited as a top layer deposited on ZrO_2.

AKNOWLEDGMENTS

Firstly, I express my gratitude to Professor Qiaoqin Yang for her role as supervisor and accepting me as her student. In her role as my supervisor, she provided excellent support, mentorship, and understanding during my master's degree.

I would like to thank Professor Safa Kasap, Ozan Gunes, and Cyril Koughia for providing invaluable guidance in many topics throughout my studies. I also would like to thank my committee members, Professor Duncan Cree, and Professor Akindele Odeshi for their valuable advice.

I am thankful to Dr. George Belev and Nanfang Zhao for their assistance, training, and advice during my studies. I also thank Dr. Jason Maley for wide ranging training and facilitation of characterization techniques found at the Saskatchewan Structural Sciences Center (SSSC).

I would also like to thank Jesus Corona Gomez for providing day-to-day assistance in the synthesis and research of thin film coatings, and all the other colleagues I have worked with during my studies for any assistance and providing a community I could rely on.

I highly appreciate the financial support from the Natural Sciences and Engineering Research Council of Canada (NSERC), CISCO Systems Inc., and the University of Saskatchewan.

Lastly, I would like to thank my parents Bruce and Becky, my brother Russel, Madison, and all my family and friends for providing me with love, support, and guidance throughout my studies and life.

TABLE OF CONTENTS

LIST OF TABLES

LIST OF FIGURES

ACRONYMS

IMT	Insulator to metal transition
PVD	Physical vapor deposition
MIT	Metal to insulator transition
T_{lum}	Luminous transmittance efficiency
T_{sol}	Solar transmittance efficiency
CVD	Chemical vapor deposition
PECVD	Plasma enhanced vapor deposition
ΔT_{sol}	Solar transmittance modulation
TES	Transition edge sensors
$\%T_I$	Insulating state transmittance
$\%\Delta T$	Percent transmittance change
SEM	Scanning electron microscopy
RMS	Average root mean square roughness
φ_{lum}	Luminous transmittance modulation factor
φ_{sol}	Solar transmittance modulation factor
FWHM	Full width half maximum
ΔH	Hysteresis width

CHAPTER 1 – INTRODUCTION

1.1 Motivation

Advancing electronic, photonic, and optoelectronic systems is an increasingly important goal for society today. Some industries that are heavily linked to all of these include communications, defense, and computing. The importance of this field is highlighted by recent major funding towards the advancement of high-tech manufacturing in Canada ($240 million)[1], and the United States ($50 billion)[2]. Phase transition materials such as vanadium dioxide (VO_2) are a promising part of this thriving industry.

Vanadium Dioxide has been the focus of much interest since it was first observed to display phase changing properties by Morin in 1959 [3]. Research on VO_2 has been focused on both the phase transition, applications in optics, electronics, optoelectronics, and the modification of the transition to suit different applications. The insulator to metal transition (IMT) of VO_2 is attractive for many uses due to the relatively low transition temperature, high transition speed, reversibility, and large change in optical and electrical properties.

Some of the most important applications of VO_2 have included optical and electrical switching [4], [5], [6], [7], [8], [9], smart windows [10], [11], [12], [13], [14], [15], [16], chemical sensors[17], [18], [19], and smart radiator designs[20], [21], [22], [23]. All of these applications make use of the IMT properties of VO_2. In smart windows and smart radiator designs, the IMT is utilized to control the temperature of buildings, and small satellites respectively. In sensing and switching applications, VO_2 phase transitions are used to change and send signals in larger systems.

These applications require some modification of pure VO_2 to better meet their requirements. Two of the most common techniques to alter the IMT behavior of VO_2 are elemental doping, and electric/optic device design. With techniques like these, the transition, optical, and electrical properties can be optimized to suit specific applications. Stacking multiple oxide layers is a common method in optic device design.

Zirconia (ZrO_2) shows promise to use an accompanying oxide layer with thermochromic VO_2 based designs due to its high thermal stability, and compatible crystallographic orientation with

VO_2. ZrO_2 also has an appropriate refractive index that enables multilayered interference designs to be made when combined with VO_2 layers. Understanding the synthesis and effects of combining ZrO_2 layers with VO_2 layers using reactive magnetron sputtering can help further understand and improve the modification and utilization of VO_2 thin films.

1.2 Objectives

The main objective for this thesis work is to investigate the compatibility of ZrO_2 with VO_2 in layered designs deposited by reactive magnetron sputtering. Different designs will show changing structural, optical and transition properties, and may be suited to different applications. Specific objectives to achieve this goal are as follows:

1. Deposit bi-layer and triple-layer oxide films with ZrO_2 and thermochromic VO_2 based layers using reactive magnetron sputtering.
2. Investigate structural properties of deposited films using Raman spectroscopy, scanning electron microscopy, and profilometry.
3. Investigate the optical and transition properties of deposited films using spectrophotometry.
4. Draw connections between deposition processes, thin film structures, and optical/transition properties of the deposited films.

1.3 Thesis Organization

In Chapter 1, the motivation and objectives for this present research, and the organization of this thesis are presented

In Chapter 2, reviews of the important aspects of the VO_2 phase transition, followed by a brief outline of ZrO_2 and its uses as a thin film are done. Next, applications of VO_2 in thin film technologies including smart windows, radiative cooling for small satellites, and sensing devices are reviewed. Modifications of VO_2 transitions by both doping, and device design are then explored further.

In Chapter 3, the process to both form and characterize thin film samples used in this study is explained. This begins with the PVD process, followed by brief explanations of Raman spectroscopy, profilometry, SEM imaging, and optical testing using spectrophotometry.

In Chapter 4, the results of the characterizations of the prepared thin films, relating the processing, structural aspects, and phase changing optical properties of the VO_2 based thin film samples are presented and discussed.

In Chapter 5, a summary of the main conclusions drawn from the results in chapter 4 and some different possible outlines of future work stemming from this study are provided.

CHAPTER 2 – LITERATURE REVIEW

Vanadium Dioxide (VO_2) has been the focus of much interest since it was first observed to display phase changing properties by Morin in 1959 [3]. This transition behavior sees large changes in optical and electrical properties of VO_2 thin films. Many applications of this phase transition have been a focus of research in both optical, electrical, and even radiative uses. In most applications, VO_2 is modified to have the desirable properties to meet the performance requirements, with doping and device design being the most common modification techniques. This chapter will first explore VO_2 phase transition, and synthesis of VO_2 films. After that, ZrO_2 as a thin film, common applications of VO_2, and the modification of VO_2 phase transition will be reviewed.

2.1 Overview of Vanadium Dioxide

Elemental Vanadium is a transition metal with atomic number 23 and is found in the group 5 transition metals. It has an electron structure of [Ar] $3d^3$ $4s^2$ with 5 valence electrons. When combined with oxygen, vanadium can show many valence levels and create multiple different oxide forms, which are shown in Figure 2.1 [24]. The most relevant portion of the V-O Phase diagram is the collection of oxides containing VO_2, V_4O_7, V_5O_9, V_7O_{13}, V_8O_{16}, V_3O_7, and V_2O_5. The small change in oxygen content between different valence states in this section of the phase diagram illustrates the difficulty that can be had when trying to form a specific desired oxidation state such as VO_2 [25], [26], [27].

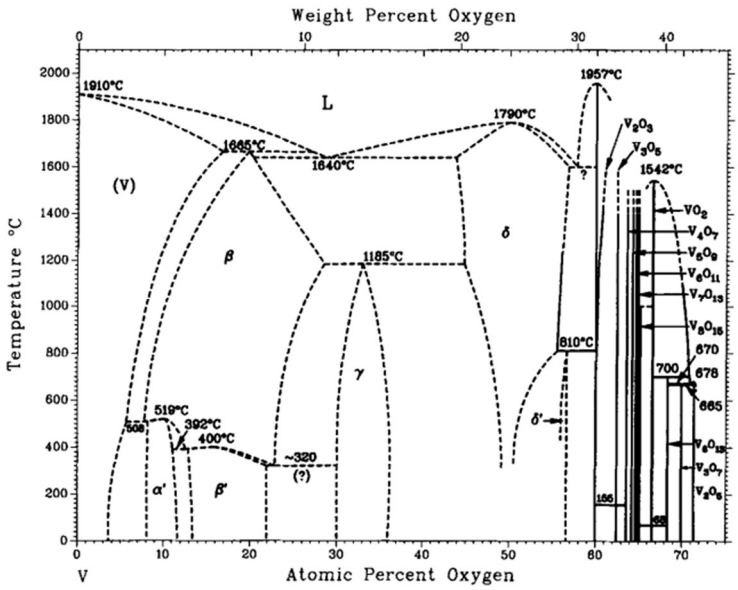

Figure 2.1: V-O Phase Diagram [24]

VO_2 has been the focus of much research due to its reversible metal to insulator transition (MIT) which occurs near room temperature [3], [25], [26], [27], [28], [29]. This transition sees the metallic rutile structure with cell parameters $a = b = 0.455$ nm, $c = 0{,}286$ nm, in the space group of P42/nm (No. 136) transition into a monoclinic insulating phase with cell parameters $a = 0.575$ nm, $b = 0.452$ nm, and $\beta = 122.6°$ [29]. These structures are shown in figure 2.2.

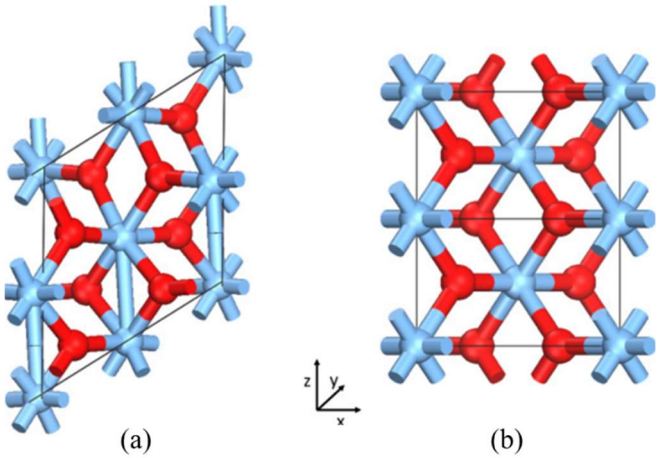

Figure 2.2: Structures of monoclinic insulating phase (a) and tetragonal rutile phase (b) [30]

There has been much debate on the specific mechanism of this process with two theories outlining the most important aspects of the mechanism by Peierls [31] and Mott [32]. The Peierls

process proposes that during cooling, the energy released by the creation of a band gap overcomes the resistance to lattice distortion, causing the shift from the rutile conducting phase to the insulating monoclinic phase [29]. This process has been confirmed in some research [33], [34], but leaves unaccounted phenomena that has been observed in the VO_2 transition. These include the experimental band gap of 0.6 eV in insulating VO_2 [35], certain magnetic properties [36], and intermediate phases that have been observed [37]. The Mott transition process includes additional considerations between different spin electrons in the d/f bands. Research of the VO_2 transition has shown evidence of a combined process that is due to both the phonon-lattice and electron-electron interactions that can better explain some of the peculiarities of the VO_2 transition.

Past research on VO_2 thin films at the University of Saskatchewan has been focused on the formation and phase transition properties of high-quality single-layer VO_2 films. Investigations into physical vapor deposition (PVD) deposition of VO_2 films have included effects of deposition parameters such as substrate temperature [38], substrate biasing [39], and vanadium pre-seeding [40] on structural, optical, and electrical properties of VO_2 thin films. The formation of different vanadium oxides through oxidation of vanadium thin films and reduction of V_2O_5 has also been studied. Single crystal VO_2 microrods have been synthesized and their transition properties have been studied [41], [42].

Studies on multilayered thin films with additional oxide layers with VO_2 have not been studied at the University of Saskatchewan. As layered structures like these are a regular part of more complex designs for specific applications, it is important to understand the effect of multilayer deposition processes and layer structures on the properties of VO_2 thin films.

2.2 Review of Zirconium Oxides

ZrO_2 was first synthesized in 1789 and had initial uses in the early twentieth century as a refractory ceramic, and as an alternative to tungsten filaments in lighting applications [43]. ZrO_2 filament lights were designed by German physicist Walther Nernst and were produced in multiple countries due to their high efficiency and resiliency [44]. ZrO_2 has been deposited as a thin film using reactive PVD [45], sol-gel deposition [46], and Pulsed laser deposition [47]. Currently, Zirconium dioxide use is widespread as it has high hardness and is thermally and

chemically stable. Application examples that incorporate ZrO_2 include thermal shielding [48], [49], [50], high performance milling tools [51], [52], [53], [54], and radiation shielding coatings [55], [56].

Thin crystalline ZrO_2 films have also been studied as optical coatings [45], [47], [57], [58] and as solid-state memory devices [59], [60]. ZrO_2 films prepared by post annealing PVD deposited Zr films in an oxygen atmosphere have shown high transmittance, refractive indexes ranging from 2.04 to 2.14, and low roughness values ranging between 1.42 and 2.28 nm. Their transparency increased, and refractive index decreased with the increase of post annealing times at 450°C. Figure 2.3 shows the resulting changes of these properties with oxygen annealing time [45].

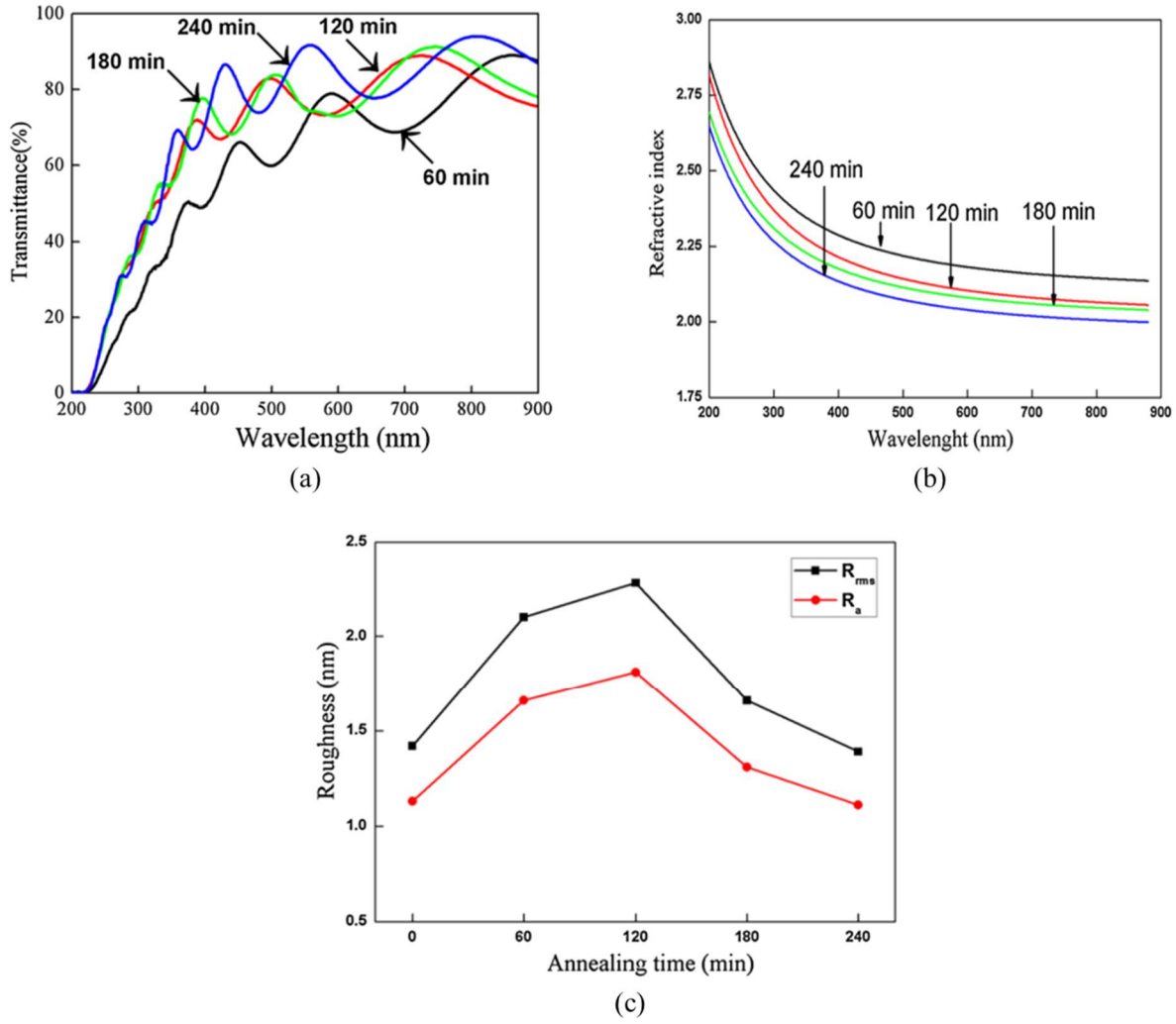

Figure 2.3: Transmittance (a) and refractive index (b) with quartz as substrates and roughness (c) with Si substrates of annealed ZrO_2 thin films [45]

There is limited research on using ZrO_2 to modify the properties of VO_2 thin films. ZrO_2 has shown promise to be used as a buffer layer, in which it has been observed to increase the transmittance [47], [58], and to decrease the transition temperature by 12-15 °C depending on the buffer layer thickness [47]. These studies utilized glass as substrates and did not achieve zero transmittance during the IMT of VO_2. Zong et al. found that increasing ZrO_2 buffer layer deposition temperature to 550 °C using the Pulsed Laser Deposition (PLD) process decreased hysteresis width, where buffer layers deposited below 550 °C showed little effects [61]. Zong et al. [58] has also deposited thin films combining VO_2 with ZrO_2 as a sandwich structure ($ZrO_2/VO_2/ZrO_2$) and bi-layer (ZrO_2/VO_2) structure using PLD. In their sandwich structure samples, an extra phase of V_2O_3 was found, which increases the transmittance in insulating and metallic states. Figure 2.4 shows the transmittance spectra of the VO_2 based thin films with bi-layer (a) and sandwich layer (b) structures. These layered structures show promise in applications that do not require zero transmittance when VO_2 is in a metallic state such as smart windows. To further this point, luminous transmittance efficiency (T_{lum}) and solar transmittance efficiency (T_{sol}) values were determined in this study. T_{lum} describes human vision efficacy and relates to transmittance in the 380 – 780 nm range, while T_{sol} describes solar transmittance through a given coating. For smart window applications T_{lum} is desired to be high before IMT and to have a minimal drop in values through the IMT, and T_{sol} is desired to have a large drop in values through the IMT. In this research, Zong et al. shows that, all the different bi-layer and sandwich structures had improved the T_{lum} and T_{sol} performance compared to the single-layer VO_2. The best performing coatings were sandwich layers with outer ZrO_2 layer thicknesses less than 200 nm and bi-layer samples with a 120 nm thick ZrO_2 buffer layer. It should be noted that no VO_2/ZrO_2 layer structures with near-zero transmittance after IMT has been reported.

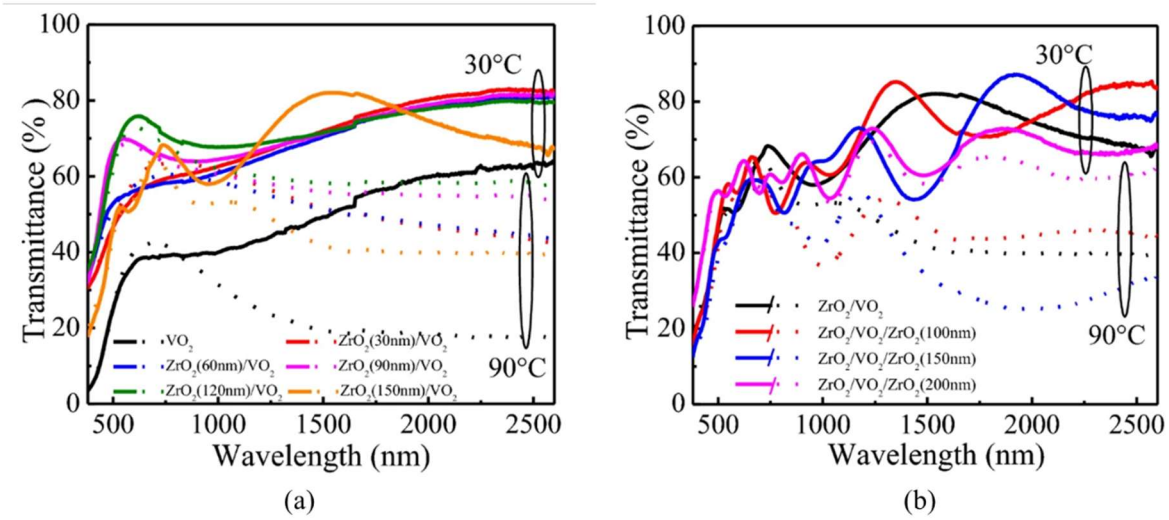

Figure 2.4: Transmittance spectra of bi-layer (a) and sandwich structure (b) films with VO_2 and ZrO_2 layers on glass substrates [58]

2.3 VO_2 Thin Film Preparation

VO_2 thin films have been prepared by many methods; some of them are summarized in table 2.1. One of the most popular methods is reactive sputtering. This process utilizes V particles sputtered from solid V target reacting with oxygen at the surface of substrate to form the desired VO_2 film. To sputter the target material, plasma is formed from an unreactive gas, the ions in the plasma are then accelerated towards the target, and the ion bombardment on the target releases target material into the chamber, which is directed towards to the substrate. Usually, Ar gas is used as it has a desirable cost and sputtering efficiency.

In the case of deposition of oxide thin films, either an oxide [62], or metallic target is sputtered with oxygen introduced into the deposition chamber [26], [27], [63]. The substrate is heated in both cases, which allows the formation of the oxide film from either the sputtered metallic atoms/ions and oxygen, or the sputtered oxide particles. The main parameters that need to be controlled during the sputtering process are target bias voltage, substrate temperature, sputtering to reactive gas ratio, and chamber pressure. Because vanadium oxides have many different oxidation levels, it is important to have a high degree of control over these parameters to successfully obtain single-phased VO_2 thin films.

In the case of pulsed laser deposition, much of the process is similar, but instead of utilizing impinging ions of a plasma to evaporate a solid target, a pulsed laser is used. In chemical vapor deposition (CVD) and plasma enhanced CVD (PECVD) processes, gaseous precursors are used, which chemically react with each other to form a desired oxide film on the substrate. Sol-gel deposition forms uniform spherical particles from a metal alkoxide solution, which is then applied to the substrate and heat treated to form a desired thin film.

Table 2.1: Summary of VO_2 thin film preparation methods

Preparation method	Application of research	Author
Reactive sputtering	Structural Study	Zhang et. al [64]
PLD	Synthesis Techniques	Lafane et. al [65]
PECVD	Synthesis Techniques	Vernadou et al. [66]
Sol-gel	Optical and transition investigation	Li et al. [67]

2.4 Applications of VO_2

VO_2 has a wide range of potential applications due to its phase changing at relatively low temperatures. Applications utilizing optical and electrical changes during the IMT/MIT in VO_2 thin films are the most common and will be the focus of this section. Specific applications that will be explored in this section include smart windows, smart radiators for satellites, and optical/electrical switching.

2.4.1 VO_2 In Smart Window Designs

Cooling of both residential and commercial buildings has become a concern due to high energy requirements [68], [69], [70], [71]. In 2023, the United States had 10% of total energy usage dedicated to cooling of both and residential and commercial buildings [71]. Global indoor cooling needs are expected to continue to rise into the future [69]. Some proposed solutions for saving energy in buildings include building integrated photovoltaic facades [72], [73], integrated green spaces [74], and use of natural lighting [75].

VO_2 shows promise for assisting these existing solutions in reducing building energy requirements. Due to its sharp change in optical properties, VO_2 has been the subject of significant research in smart window applications [10], [11], [12], [13], [14], [15], [76], [77], [78]. A smart window design utilizing VO_2 would automatically decrease the incoming thermal energy as the temperature of the window rises and VO_2 undergoes its IMT. Figure 2.5 below shows a smart window design (a) and an experimental set up (b) and impact on internal temperature (c) for testing a smart window with a VO_2 layer [10]. It can be seen that VO_2 is effective in lowering the internal temperature of the set up once the outer window temperature reaches the transition temperature.

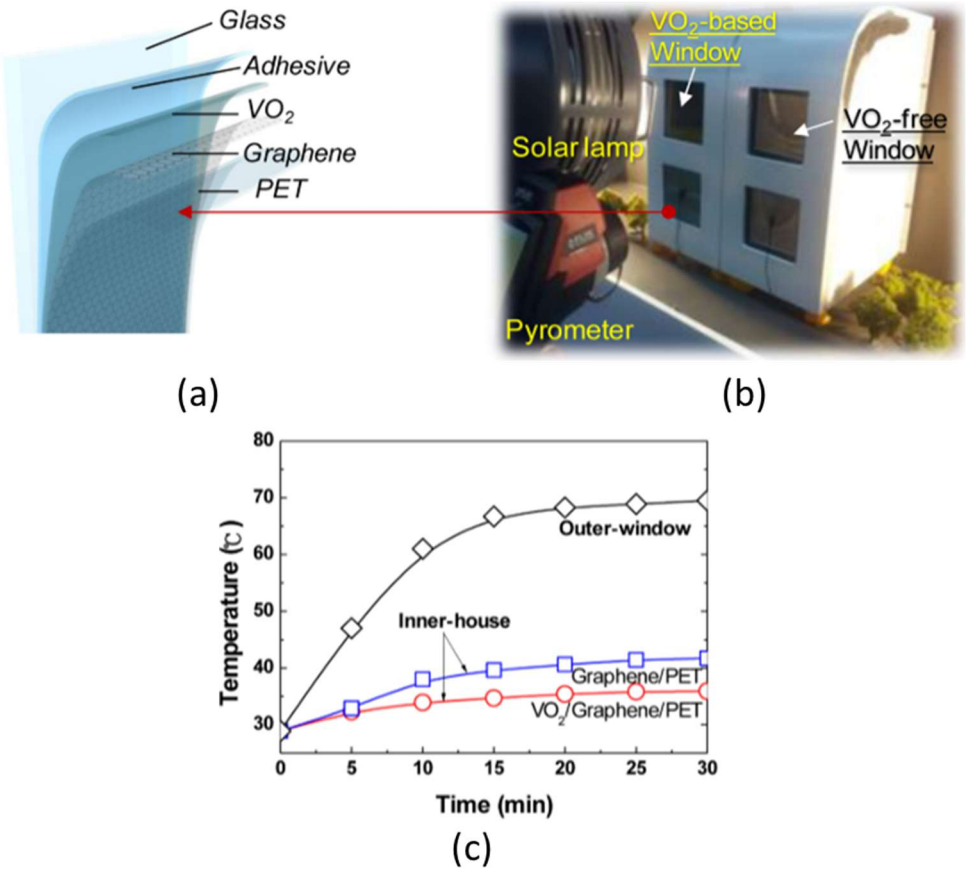

Figure 2.5: Experimental design (a), testing set up (b), and temperature results (c) of a VO_2 based smart window [10]

Two of the most important parameters for VO_2 in smart window designs are the transition temperature, and transmittance spectra above and below the transition temperature. For smart

window applications, the transition temperature is aimed to be lowered from 69 °C. For optical properties, it is desired to have a high luminal transmittance of wavelengths in the 380-780 nm range (T_{lum}) before and after the IMT, and a high modulation of incoming solar energy which is the change in transmittance for wavelengths within the range of 240 – 2500 nm (ΔT_{sol}) [79]. Specific methods for calculating these parameters are presented in section 4.2.1 when discussing T_{sol} and T_{lum} of samples prepared in this thesis.

To lower the transition temperature and improve the optical performance of VO_2 smart window designs, doping[11], [13], [76] and layer/film designs[10], [11], [12], [14], [15], [16], [80], [81] are the most common techniques. Examples of doping with Al (a) and layer design (b) can be seen in figure 2.6 [63], [76]. Both examples display increased transmittance, and Al doping is shown to decrease the transition temperature compared to the corresponding pure VO_2 films.

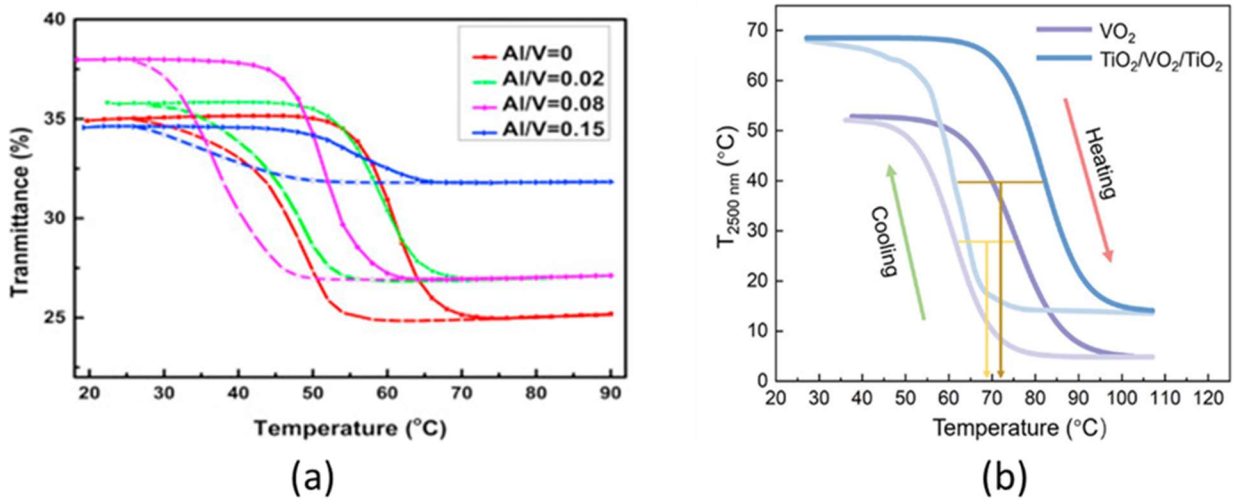

Figure 2.6: Effect of Al doping [76] (a) and TiO_2 layer design[63] (b) on VO_2 for smart window applications

To be utilized on an industrial scale, the manufacturability of VO_2 films must be improved. As reviewed in the previous section, vanadium has many oxidative states within very close margins, and is easily oxidized [24]. As V_2O_5 and V_2O_3 particulates have been shown to be toxic [82], [83], [84] , it is even more urgent to achieve large scale manufacturing of pure VO_2. As VO_2

usually has a brown tint, some regions may see a need to adjust the color, and this can also be achieved by doping and multilayer designs [79].

2.4.2 VO2 in Satellite Applications

Spacefaring systems have unique operating environments in which they can be exposed to high thermal fluctuations [85], [86], [87], [88] with the majority of heating coming from thermal radiation. Temperatures can see large variations between their illuminated sides [85] and between the whole system when in the shade of the earth [89]. Figure 2.7a and 2.7b show a summary of incoming heat acting on an orbiting satellite [90] and a simulation of temperature fluctuations in a rotating spacecraft at different angular velocities [85] respectively.

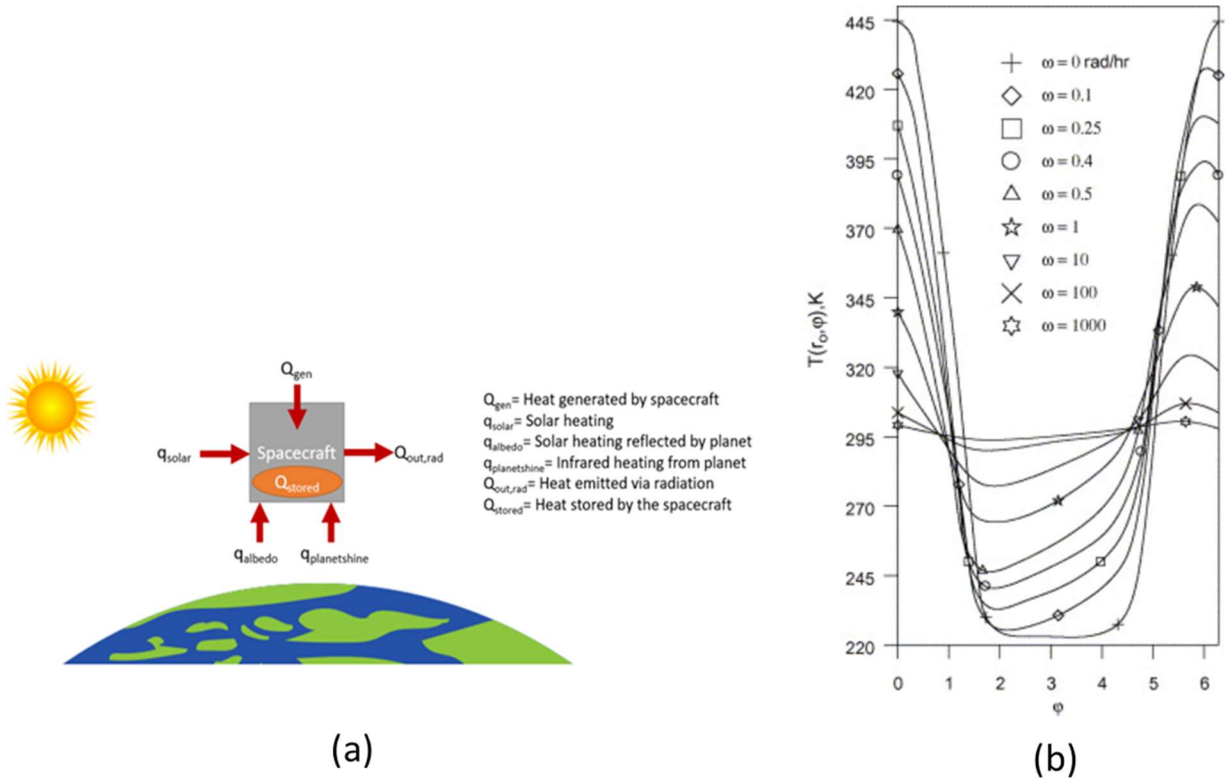

Figure 2.7: Heating Sources on an orbiting satellite [90] (a), and a simulation of temperature change in a rotating spacecraft [85] (b)

A pervasive issue with satellites is keeping sensitive instruments in their desired temperature range. Large spacecraft and satellites can use complex thermal management systems including capillary pumped loops and loop heat pipes [91] while small satellites have limited space for

complex thermal management [90]. Without relying on internal cooling cycles, spacecraft must rely on controlling radiative cooling. To quantify this, emittance is used, which is defined by the ratio of the radiation of a given surface to a blackbody (ideally radiating surface) at the same temperature [92].

VO_2 has many useful characteristics for smart thermal management in satellite and spacecraft applications. The most obvious one is the sharp, reversable change in reflectance to deal with highly direction and position dependent heating in a space environment. VO_2 also has the advantage of being able to survive in the space environment while being highly tunable with doping and multilayer designs.

Most applications of VO_2 in spacecraft utilize switching effects to produce variable emittance radiator designs [20], [21], [22], [23], [89], [93], [94]. These designs utilize reflection interference structures to have high emittance when the VO_2 layer is in a metallic state and high absorption while in an insulating state. Figure 2.8 shows a schematic of a usual resonance structure with insulating state (a) and metallic state (b) VO_2 layers [23].

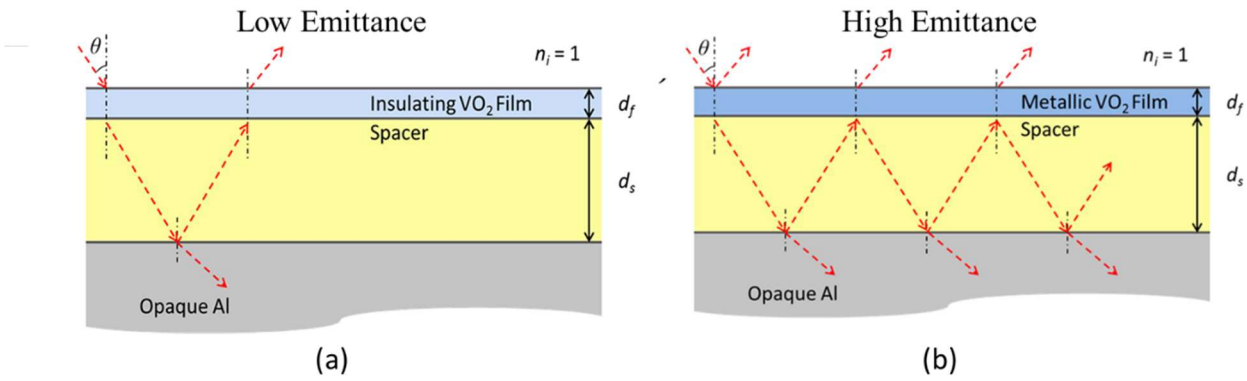

Figure 2.8: Variable emittance resonance design for smart radiator [23]

Smart radiating designs have an exterior thermochromic VO_2 layer, followed by a spacing layer, deposited on a highly reflective base which can be either a thin metallic layer or a metallic substrate. Spacing layers that have been used include SiO_2 [20], [21], [22] and BaF_2 [89]. Doping of the VO_2 layer has also been utilized to control the transition temperature to the desired ranges [22].

By altering the thickness of two outermost layers, radiation and reflection can be tuned for temperatures above and below the transition of the VO_2 layer. Layer designs are usually tuned to have high emittance centered at the 10 μm wavelength to have maximum emittance of solar radiation. Variable emittance designs have been shown to increase radiative power by 38% to 49% [20], [21], [22], [23], [89], [94] when above the transition temperature. An example of the change in emittance (a) and radiative power (b) is shown in figure 2.9 [23].

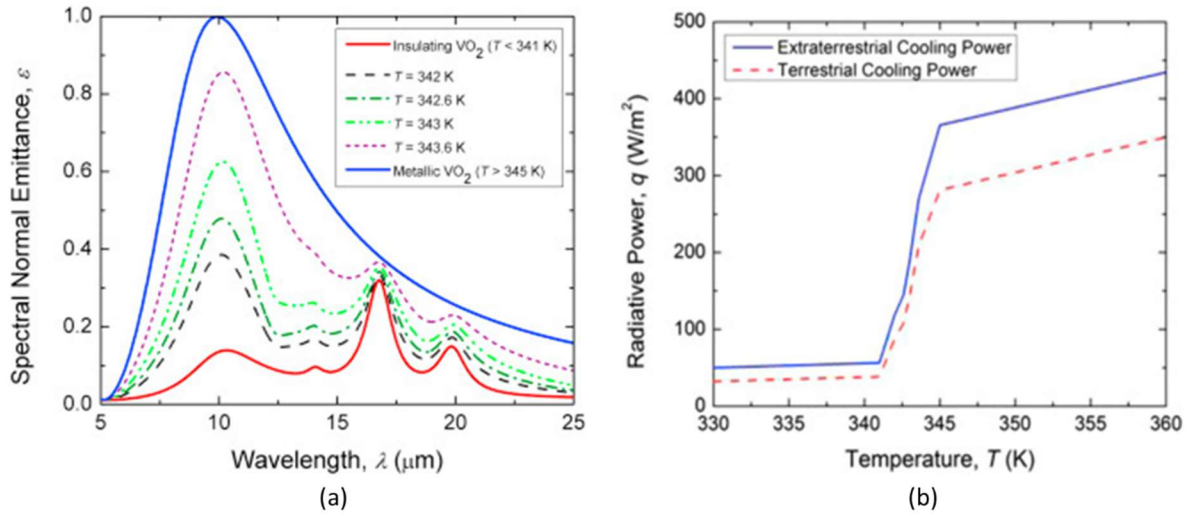

Figure 2.9: Change spectral emittance (a) and change in total extraterrestrial radiative power of a VO2 based variable emittance design [23]

VO_2 based smart radiator designs show effective cooling for lightweight compact systems, useful especially for small satellites. There is usually a need to adjust the transition temperature and manipulate incoming light to best meet the desire performance. This highlights the importance of research into layer compatibility and design.

2.4.3 VO_2 in Sensing and Switching Applications

Sensors and switches both can utilize the VO_2 phase change. In a simplified view, both a switch and a sensor take an input signal and change or redirect the other parts in a system. In the case of VO_2, the sensing device will be structured so that the input signal will instigate a phase change and subsequently direct a different signal in the system. For example, in a device that is used as a photodetector as shown in figure 2.10 [95], incident light will instigate the IMT which will allow a current to pass through. Incident light is a favored input as it facilitates ultra-fast phase

transitions [4], [96], [97]. IMT instigating input signals can be varied to fit different applications, specific examples are further outlined in this chapter. VO_2 phase transition can be applied in traditional data transfer and computing using optoelectronics [98] as well as neuromorphic devices [99]. The main advantages of VO_2 for switching and sensing applications include reversibility, speed, and tunability of the VO_2 transition.

Kabir et al. developed a simple two terminal planar photodetector design using VO_2 deposited with reactive sputtering. They found high detection performance with significant increase in illuminated current with metallic phase VO_2 [95]. This design and photo response can be seen in figure 2.10. This shows promise for uses as wide range photodetectors with the further ability to tune responses based on device temperature.

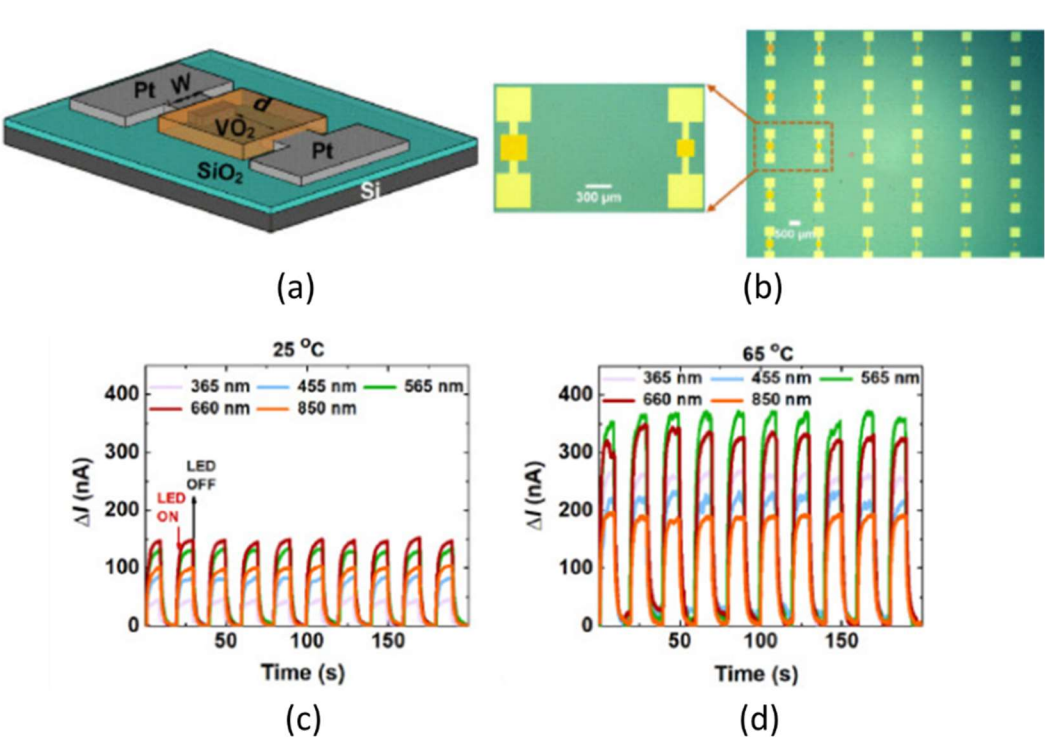

Figure 2.10: Planar VO_2 based photodetector Schematic (a) and optical image (b), and current response from LED illumination at different wavelengths at 25 °C (c) and 65 °C (d) [95]

For many VO_2 applications, modified layer and device design can result in further control of optical performance. In their paper, Song et al. [7] used silver nanoparticles to create selectively low reflection at certain wavelengths. They found that by altering the spacing between silver

nanoparticles, they could selectively filter to gain high photodetection at different wavelengths. The design and resulting reflectance spectrums can be seen in figure 2.11[7].

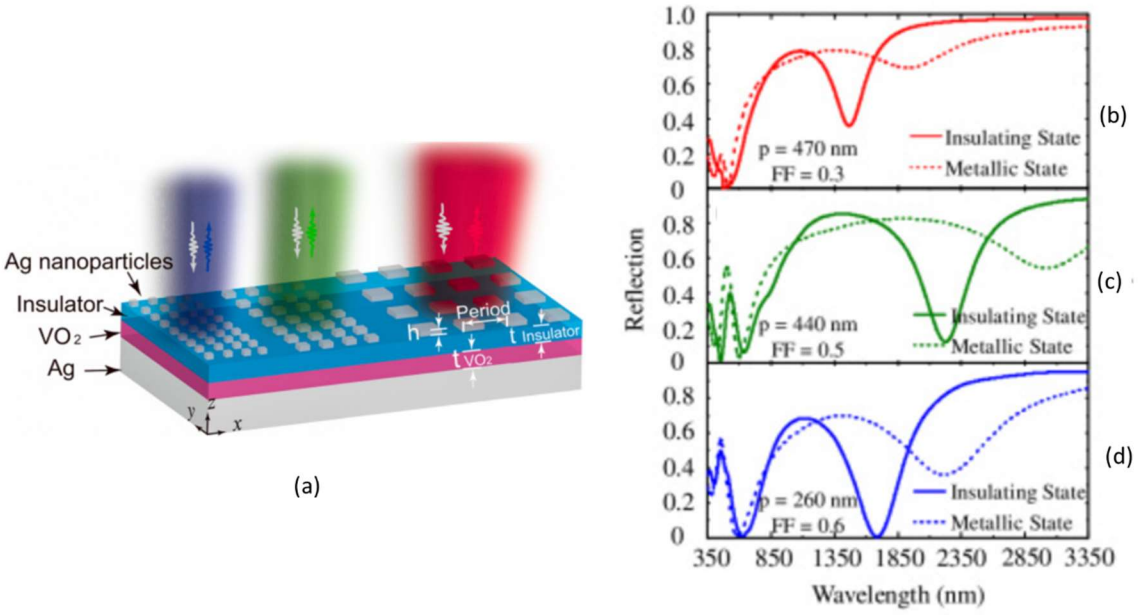

Figure 2.11: Design of variable reflectance VO_2 based Photodetector (a), and reflectance spectrums of designs with 470 nm (b), 440 nm (c), and 260 nm (d) spacing [7]

While the VO_2 phase transition is most used in manipulating photo or electrical signals, it can also be used as gas sensors. Lin et al [19] modeled the adsorption reaction of a VO_2 monolayer, with H_2O, CH_4, and CO as an optical gas sensing material. They found that CO showed the greatest change in optical properties after adsorption. Hydrogen detection has been studied in VO_2 nanobelts [100] and Pd enhanced nanowires [101], and both show high performance. Pd enhanced nanowires and their hydrogen detection can be seen in figure 2.12 (a) and (b) respectively [101].

Another unique gas sensing set up was made by Strelcov et al. [102]. Their sensing device was inspired by transition edge sensors (TES) utilizing superconducting materials. The main idea of a TES is to bring a given material very close to the threshold of electrical transition where the interaction of gaseous molecules can trigger the transition and see a large change in electrical properties. In the case of superconductors, this threshold is at a very low temperature [103],

which can be prohibitive in practical and research applications. For VO_2, the transition threshold is at a much more easily obtained temperature. Using a nanowire set up shown in Figure 2.12c and 2.12d, Strelcov et al. were able to successfully detect H_2, He, air, and Ar gases.

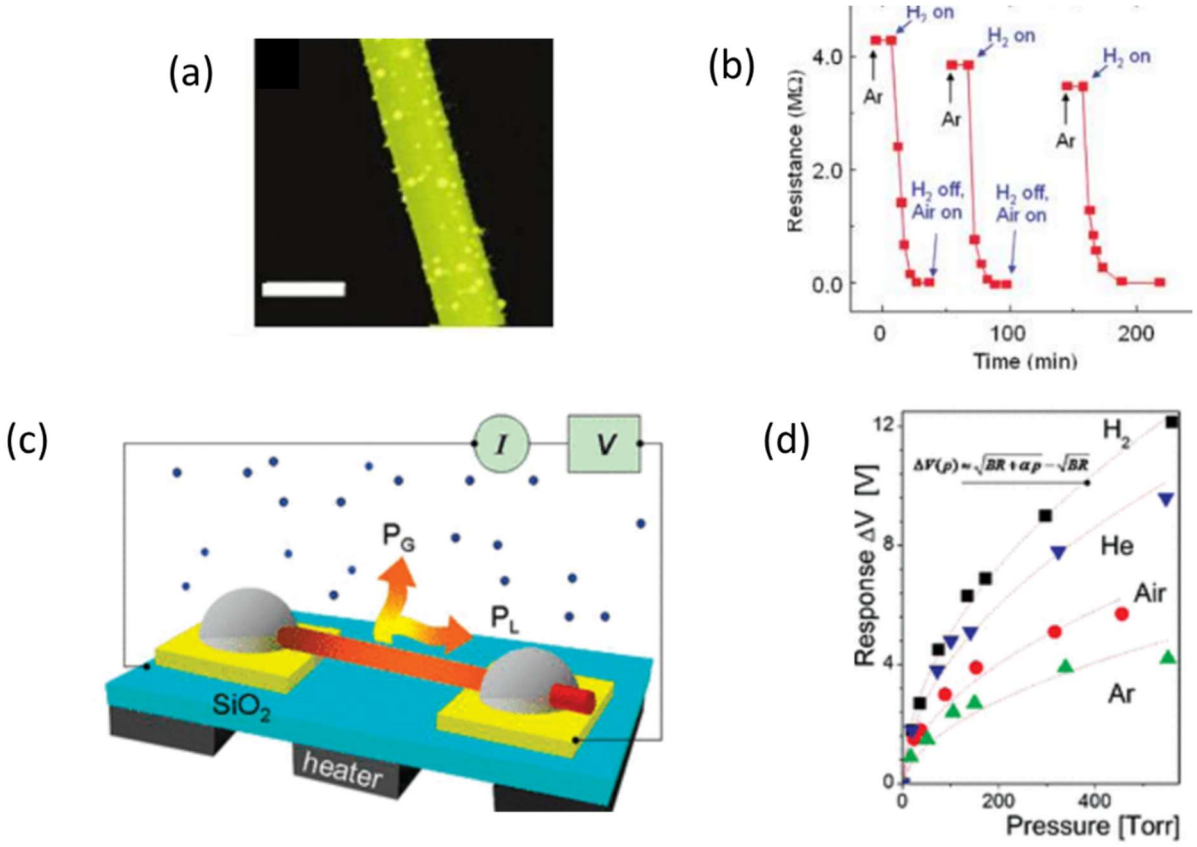

Figure 2.12: Pd enhanced VO_2 nanowire (a) and the corresponding resistance response to hydrogen (b) [101], and nanowire two terminal sensor set up (c) with the resulting voltage response to different gas pressures (d) [102]

Optical and electrical sensing applications follow the pattern outlined in other examples of VO_2 applications. This pattern being the utilization of the IMT switching behavior as part of more complex designs. Many of these designs include 2-D stacks with VO_2 layers with other modifications such as doping.

2.5 Modification of VO_2 thin films

As seen in section 2.4, most potential applications that utilize the IMT behavior of VO_2 need to adjust the transition and/or optical properties. The main strategies for modifying the optical and electrical behavior of VO_2 are elemental doping and optical/electrical device design. These can effectively produce designs capable of meeting many different design requirements.

In smart window applications, doping is generally used for reducing the transition temperature, and increasing luminous transmittance (T_{lum}) and solar modulation (ΔT_{sol}) which are described in more detail in section 2.2.1. Dopant elements including W, F, Mg, Sr, Ba, Nb, Mo, and Zr have been studied and the results show doped VO_2 with improved properties for various applications. Table 2.3 summarizes the effect of doping on properties of VO_2 films. W has been especially well studied and shown to decrease the T_{IMT} and improve T_{lum} and T_{sol}. For optoelectrical switching applications, it is desirable to have a high transmittance in an insulating state ($\%T_I$) and a change in transmittance following the IMT $\%\Delta T$. Tuning VO_2 for switching applications may also include the tuning of the optical properties at specific wavelengths, which is mainly achieved by device/layer design, but element doping such as Al has been shown to be able to achieve this as well. A summary of different dopants and their effects can be found in table 2.3.

Table 2.2: Summary of VO_2 modification through elemental doping.

Dopants	Concentration	Effect(s)	Application	Reference
W	0.5 – 2 at.%	Decrease T_{IMT} (29C°)	Smart Windows	Hu et al. [104]
W	0.5 – 2.3 at.%	Decrease $\Delta\%T$, T_{MIT}, hysteresis width	Electrical Switching	Ivanov et al. [105]
W	-	Decrease $\%T_I$, T_{MIT}	Smart Windows	Outon et al. [11]
W	0.5 – 2 at.%	Decrease $\Delta\%T$, T_{MIT}, Decrease in hysteresis width	General	Chen et al. [106]
W	0.8 at.%	Modified heat transfer properties (α, ϵ, k, C_p), Decrease T_{MIT}	General	Gomez-Heredia et al. [107]
W*[1]	0.2 – 2 at.%	Decrease $\%T_I$, T_{MIT}		Hu et al. [104]

Mg	1.9 – 20 at.%	Increase $\%T_I$, Decrease Δ%T	Smart Windows/ General	Dietrich et al. [108]
F	0.37 – 2.93 at.%	Decrease T_{IMT} (35C°), color adjustment	Smart Windows	Dai et al. [109]
Ca	1.3 – 8.5 at.%	Increase $\%T_I$, Decrease Δ%T, T_{IMT}	Smart Windows/ General	Dietrich et al. [108]
Sr	1.4 – 9.7 at.%	$\%T_I$, Decrease Δ%T, T_{MIT}	Smart Windows/ General	Dietrich et al. [108]
Ba	4.7 – 11.4 at.%	Increase $\%T_I$, Decrease Δ%T, T_{MIT}	Smart Windows/ General	Dietrich et al. [108]
Nb	2.6 – 3 at.%	Decrease $\%T_I$, T_{MIT}	Smart Windows/ General	Piccirillo, Binions, Parkin. [110]
Mo	0.6 – 2.1 mol%	Increase $\%T_I$, Decrease Δ%T, T_{MIT}	Smart Windows	Suzuki et al. [13]
Zr	4.2 – 9.8 at.%	Increase $\%T_I$, Decrease T_{MIT}, Color adjustment	Smart Windows	Shen et al. [111]
Co	2.0 – 8.0 at.%	Decrease Δ%T, T_{MIT}	Optoelectrical Switching	Lu et al. [112]
Y	3.30 – 3.48 at.%	Decrease Δ% Resistivity, Increase in hysteresis width	Electrical Switching	Zhou et al. [113]
Gd	-	Decrease Δ% Resistivity, band gap, Decrease in hysteresis width	Electrical Swithching	Gu et al. [114]
Al	-	VO_2(M) formation, Decrease %T at 800 nm wavelength	General	Wang et al. [115]
Ge	5 at.%	Increase T_{MIT},	Electrical Switching	Muller et al. [116]

Mg/W	0.0/2.1 – 5.3/2.1 at.%	Increase $\%T_I$, Decrease Δ%T, T_{MIT}	Smart Windows/ General	Wang et al. [117]
F/Mo	<0.1/0.3 - <0.1/2.3 mol%	Increase Δ%T, Decrease, T_{MIT}	Smart Windows	Suzuki et al. [13]
W/Zr	0.6/8.5 – 2.4/8.5 at.%	Decrease T_{MIT} (29 C°),	Smart Windows	Shen et al. [111]

* denotes that there is additional structural changes other than doping

*[1] porous grain structure

For most applications of VO_2, there is an advantage to including additional layers, which allows for the modification of the optical properties of devices to better use the VO_2 phase switching. In smart window designs, it is common to add layers to control the transmittance of sunlight more effectively and optimize T_{sol}, and T_{lum} [76]. More inert outer layers are also utilized to make more robust designs to last on large buildings [15]. In Smart radiator designs, additional layers are used to increase emittance [23]. For electrical and optical switching and gas sensing applications, there is a need for the addition of extra structures to enable different functionalities [100], [101], [102].

Applications that have been explored in this review regularly use additional oxide layers to achieve desired optical and transition properties. This suggests the need for further study into the formation of thermochromic VO_2 based thin films that utilize additional oxide layers. ZrO_2 has been chosen for this study as it has compatible optical and structural properties to utilize with VO_2. There has also been limited research into films that combine ZrO_2 and VO_2 layers that reach full transition upon heating.

CHAPTER 3 – MATERIALS AND METHODS

This section will outline the processes in which thin film samples were designed, made, and tested. The first section will outline the deposition system and general process used in the synthesis of thin film samples. Films in this study were deposited using reactive magnetron sputtering deposition technique. To characterize the structure of deposited samples, Raman spectroscopy, scanning electron microscopy (SEM), and optical profilometry were used. Optical characterization with spectrophotometry were used to test the optical properties before, during, and after the IMT phase transition.

3.1 Synthesis of Thermochromic VO_2 Based Thin Films

A SPT320 sputtering system made by Plasmonique Inc. was used to prepare thin film samples. The table below outlines the relevant features of the system from its manual [118] and figure 3.1 is a simplified schematic of the SPT320 system. Metallic vanadium and Zirconium targets used in the deposition of multilayered coatings were 2 inches in diameter and 0.25 inches in thickness with 99.99% purity supplied by Plasmonique Inc. Substrate materials included mirror polished (100) Si and R-cut sapphire.

Table 3.1: SPT320 System Specifications

Plasma System	• Three magnetrons for 2-inch targets with shutters and shields • 1 RF generator 300W 13.56 MHz with automatic matching used for substrate biasing • One DC generator 500W • One DC generator 1kW
Vacuum System	• Turbo pump: 560L/s(N_2) on ISO-K flange • Mechanical pump: rotary vane 24m^2/hr charged with PFPE lubricant • Automatic Throttling valve

	• Capacitance monometer 10^{-5} to 0.5 Torr • Wide range gauge 10^{-9} Torr to 1 atm • Stainless steel deposition chamber
Substrate Mount	• Heating to 850 °C with PID control • Sample Rotation and vertical positioning
Gas management system	• Three mass flow controllers calibrated for available gases Ar, N_2, and O_2
Thickness measurement System	• Quartz microbalance

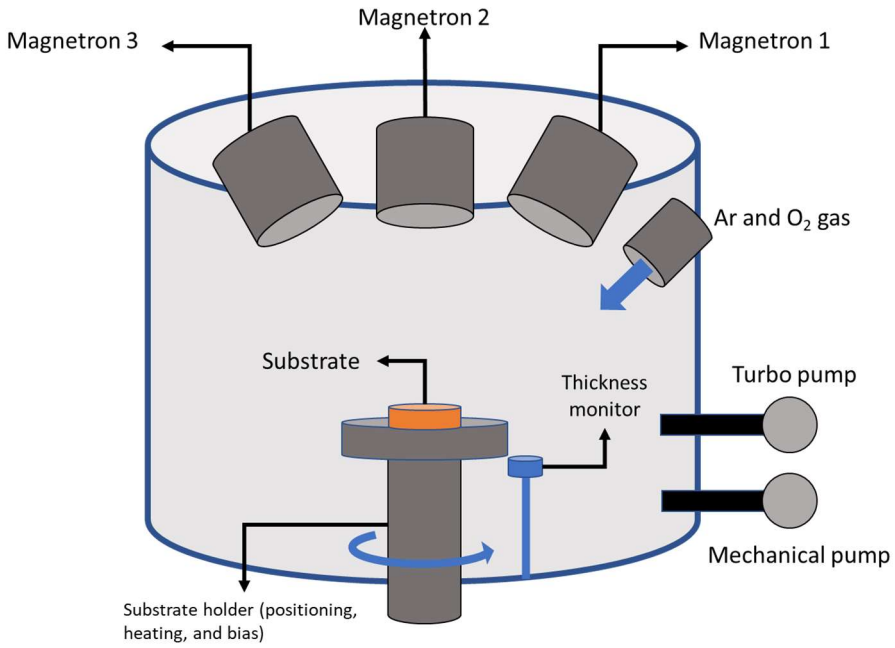

Figure 3.1: SPT320 physical vapor deposition system schematic

In this work, reactive magnetron sputtering was used to prepare oxide thin films. The reactive magnetron sputtering process begins with the introduction of argon and oxygen gas in a controlled ratio into a vacuum chamber. Power is then supplied to the solid-state targets, which forms plasma. This plasma is condensed onto the target due to the magnetron included in the

target mount, which increases sputtering rate and control. The ions in the condensed plasma are accelerated and bombard the solid-state targets to release gaseous particles. These particles then reach the heated substrate and react with oxygen at the surface to form the oxide films. Important parameters during the film deposition process include reactive/inert gas flow ratio, substrate temperature, working pressure, substrate to target distance, and deposition time. The basic operational steps for the reactive sputtering process used in the present research are outlined below.

1. Sample and chamber preparation
2. Deposition environmental set up
3. Substrate sputter cleaning
4. Reactive sputtering deposition
5. Chamber venting and specimen retrieval

Sample preparation in this work included cutting and cleaning Si and sapphire substrates into suitable sized sheets, which are at least 1 cm in width and 3-5 cm in length for fitting into spectrophotometer testing. Prior to being placed in the chamber, the substrate was cleaned using compressed air to remove the surface particles. The vacuum chamber was regularly polished and cleaned to remove the accumulated depositions from previous deposition experiments.

After the substrates are loaded into the deposition chamber, the pump system outlined in table 3.1 was used to bring the chamber to a base pressure of 10^{-6} Torr. This base pressure is much lower than the operating pressure for depositions to reduce contaminates left in the chamber during the deposition process. After the chamber reached the desired base pressure, 40 sccm of argon gas was introduced into the chamber and the pressure was set to 10 mTorr. Substrate biasing of 150 W RF was applied for 15 minutes to produce plasma which bombards the substrate surface to remove any remaining impurities. The substrates were then heated to the desired temperature for deposition. Next, the desired mixture of argon and oxygen gas flows were introduced into the chamber, and DC voltage was applied to the selected targets to accelerate the ions to have sufficient energy to sputter off the targets. The sputtered metallic particles then react with oxygen at the substrate surface to form the VO_2 and ZrO_2 films.

To better understand the effect of layered structure on the properties of the multilayered thin films combining VO_2 and ZrO_2 layers, three different layer designs were used. These include bi-layers with an alternating order of ZrO_2 and VO_2 layers, and a triple-layer sandwich structure with a VO_2 layer between two ZrO_2 layers. Examples of these structures are shown in figure 3.2. When discussing different layer structures, they will be referenced by the layers closest to the substrate first. For example, the bi-layer film with ZrO_2 deposited on top of a VO_2 layer would be described as VO_2/ZrO_2.

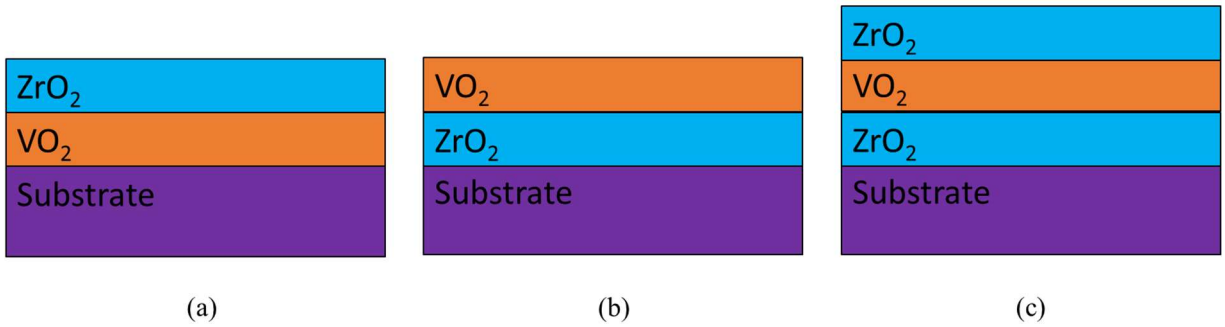

Figure 3.2: Layer structures of VO_2 based thin films samples, including VO_2/ZrO_2 (a) ZrO_2/VO_2 (b), and $ZrO_2/VO_2/ZrO_2$ (c)

For VO_2 layers, deposition parameters were based on previous research at the University of Saskatchewan which resulted in high performing single-layer VO_2 films [38]. Gas flows of 100 sccm and 1.4 sccm for argon and oxygen, respectively, were used. Sputtering power for the vanadium target ranged from 100 to 120 W DC for VO_2 layers depending on the amount of target wear. ZrO_2 parameters were initially based on previous research at the University of Saskatchewan [119], then changed to better suit this study. Specifically, the oxygen/argon ratio was lowered, and the deposition temperature was increased. Lowered oxygen/argon ratio aims to lessen the risk of oxidation in previously deposited VO_2 layers, and increased temperature is intended to limit the effects of thermal mismatch between previously deposited VO_2 layers and ZrO_2 layers. For ZrO_2 depositions, an argon flow of 50 sccm, an oxygen flow of 5 sccm and a 150 W DC sputtering power were used for sputtering the Zr target. ZrO_2 layers in the bi-layered samples and as a layer directly on the substrate in the triple-layered samples were deposited at 650 °C while the top ZrO_2 layers in triple-layered samples were deposited at 500 °C and 650 °C.

The deposition time for VO_2 layers was 2 hours and 15 minutes and for ZrO_2 layers was 1 hour and 15 minutes. Table 3.2 gives a summary of deposition parameters.

Table 3.2: Oxide Layer Deposition Parameters

Deposition Layer	Ar/O_2 gas flow (sccm)	Substrate Temperature (°C)	Deposition duration
VO_2	100/1.5	650	2 hours 15 minutes
ZrO_2	50/5	650	1 hour 15 minutes
ZrO_2 (Top of triple-layered samples)	50/5	550,650	1 hour 15 minutes

3.2 Characterization of VO_2 thin films

The structural and optical properties of the VO_2 thin film samples were characterized using various advanced techniques. The goal of this characterization is to understand the relationships among the optical functionality, structures, and processing parameters. Understanding all these different relationships will provide useful knowledge for future processing of high quality VO_2 films for specific applications. The techniques for structural tests include Raman Spectroscopy, scanning electron microscopy, and optical profiling. Optical testing with spectrophotometry was used to obtain transmittance spectra with wavelengths of 300 nm – 2500 nm for samples in their insulating state and metallic state. Samples transmittance values were also measured at the 1550 nm wavelength through the phase transition with steps of 2 °C.

3.2.1 Raman Spectroscopy

Raman spectroscopy is a characterization technique that detects inelastic scattered light from a high intensity laser light source. When the impinging light interacts with a molecule in a material, the majority of the light released from the sample has the same frequency as the incident light and is called Rayleigh scattering. A small portion of the released light with different frequency is called Raman scattering. Raman shift comes from a molecule gaining energy from the impinging light and changing its vibrational modes [120]. This takes some energy from the light which has a changed frequency (wavelength shift). This shift reflects the bonding structure of the tested molecule.

Raman Spectroscopy was used in this study to determine the vanadium oxide states present in the samples. A Renishaw Invia Reflex Microscope located at the Saskatchewan Structural Sciences Center was used. A laser source with a wavelength of 514.5 nm was used, and Raman spectra of 100 – 1800 cm^{-1} were recorded in order to capture all the possible oxidation states of vanadium oxides present. To mitigate the risk of oxidation from interaction between the film and 514.5 nm laser, the operating power was set to 50% for this work. The Raman system was calibrated to under 1 cm^{-1} error prior to each testing session utilizing an internal Si calibration.

3.2.2 Electron Microscopy

Scanning electron microscopy is a common and useful technique to observe materials' morphology. SEM uses a high energy beam of electrons focused on the testing sample, and the electron beam interacts with the sample produces different measurable signals. A summary of relevant signals is shown in table 2.3. In this research, secondary electron imaging was used to determine the thickness and layer structure of the multilayer films.

Table 3.3: Summary of common signals produced and detected in SEM

Signal	Characteristic results
Secondary electrons	Topography, magnetic state, voltage state
Backscattered electrons	Atomic number, topography, magnetic state
X-rays	Chemical and elemental analysis

A Hitachi SU8010 SEM was used in this study to observe the cross-sections of the samples. The thickness of each layer in the samples can then be determined by the cross-sectional SEM images. After samples were cut using a diamond cutting tool, the exposed cross-sections of the samples were then deposited with a thin layer of gold via sputtering deposition. This gold coating

is required for high resolution SEM imaging of insulating and semiconducting samples to ensure high conductivity, which reduces surface charging.

3.2.3 Surface Profilometry

Surface roughness measurements of the film samples deposited on Si substrates were done using a Zygo NewView 8000 optical profilometer. Average root mean square (RMS) roughness values of five surface scans were used to lessen the effects of surface imperfections for individual samples. Surface roughness has an important role in surface scattering of light which is an important consideration for optical thin films. Multilayer film designs are especially sensitive to light scattering as their function commonly relies on precise interactions and interreflections between layers which can be skewed by high roughness values between different layers. Examples of these designs include antireflection and variable emittance radiator designs discussed in section 2 of this report. In this study, profiles were taken 5 times and averaged to reduce the error.

3.2.4 Spectrophotometry

Spectrophotometry is a method used to obtain optical properties such as transmittance, reflectance, and absorbance, of a material. This data can then be combined with additional analysis to determine other important optical properties such as a materials complex refractive index, absorption coefficients, and optical band gaps [121], [122]. In spectrophotometry, an incident light is split and directed to a test sample and a reference section. The resulting intensity is then compared between the light that passes through the sample and the unchanged reference light. A Lambda 900 UV-Vis-NIR Perkin-Elmer spectrophotometer was used for this study. Before spectrophotometry testing, an internal calibration was performed to under 1% error in transmittance readings.

Spectrophotometry was used to determine the optical and transition properties of thermochromic films in this study. This system has the capability of measuring transmittance properties of the samples in a wavelength range from 1 to 2500 nm, with a deuterium lamp providing 1 – 300 nm, and a tungsten lamp providing 300 – 2500 nm incident light. In this study, only the tungsten lamp was used as the applications of thermochromic films utilize the visible (400 – 700 nm) and the near-infrared (800 – 2500+ nm) spectra. Samples were tested at room temperature and

elevated temperature above the VO_2 transition temperature over wavelengths of 300 – 2500 nm. To ensure VO_2 films had undergone a full IMT, elevated testing temperatures ranged from 80 °C to 95 °C depending on the specific samples tested.

To understand the specifics of the transition and hysteresis behavior of thermochromic films prepared in this study, an additional hysteresis test was done on each sample. This test involved measuring the transmittance values of samples at 1550 nm in 2 °C increments during a heating/cooling cycle. The 1550 nm wavelength was chosen as it is commonly used in communication systems. The cycle begins at room temperature and rises to where the IMT is fully complete, and then cools down back to room temperature. This test gives important information concerning the response speed, hysteresis, and instigation temperatures of transitions in thermochromic samples.

CHAPTER 4 – RESULTS AND DISCUSSION

In this chapter, the structural and optical testing results of the thin film samples are presented and the relationships between the thermochromic properties, layer design, and the structures are discussed.

4.1 Structural study of VO_2 based thermochromic films

4.1.1 Raman Spectroscopy

The Raman spectra of the samples deposited on Si and Sapphire with a single-layered VO_2 thin film as a reference are shown in figure 2(a) and figure 2(b), respectively. These samples show only VO_2 peaks located at 144, 193, 223, 260, 308, 334, 389, 497, and 613 cm^{-1} [27]. Bi-layered ZrO_2/VO_2 samples only show VO_2 peaks, while the VO_2/ZrO_2 samples show phases of VO_2 + V_2O_5+ ZrO_2 as the spectra display additional peaks at 145, 195, 284, 303, 405, 483, 528, and 997 cm^{-1}, which are the characteristics of V_2O_5 [27], and at 770 cm^{-1}, which is a characteristic peak of ZrO_2 [123].

For the triple-layered samples with a top layer deposited at a temperature of 500 °C, both VO_2 and V_2O_5 peaks appear. But for the triple-layered samples with a top layer deposited at a temperature of 650 °C, there is a decrease in intensity for VO_2 peaks as well as the appearance of new peaks at 167, 838, 875, 925, and 978 cm^{-1}, which are characteristics of V_6O_{13} [27]. The triple-layer samples with ZrO_2 deposited at 550 °C do not show a peak at 770 cm^{-1}, indicating 550 °C is ZrO_2 is not high enough to form a crystalline top layer of ZrO_2. The results have also shown that VO_2 layers in this study are thick enough to block the Raman peaks of ZrO_2 layers below, as ZrO_2/VO_2 and $ZrO_2/VO_2/ZrO_2$(650 °C) samples do not show ZrO_2 Raman peaks. This is confirmed by SEM imaging which show crystalline ZrO_2 bottom layers and will be outlined further in chapter 4.1.3.

It has been reported in previous research that VO_2 based films with oxidized phases such as V_2O_5 and V_6O_{13} showed increased T_{IMT} and hysteresis widths [124], [125]. This suggests that samples with ZrO_2 deposited on top of VO_2 will show these features. This will be further discussed in sections 4.2.1 and 4.2.2 when discussing transmittance and hysteresis properties of the samples.

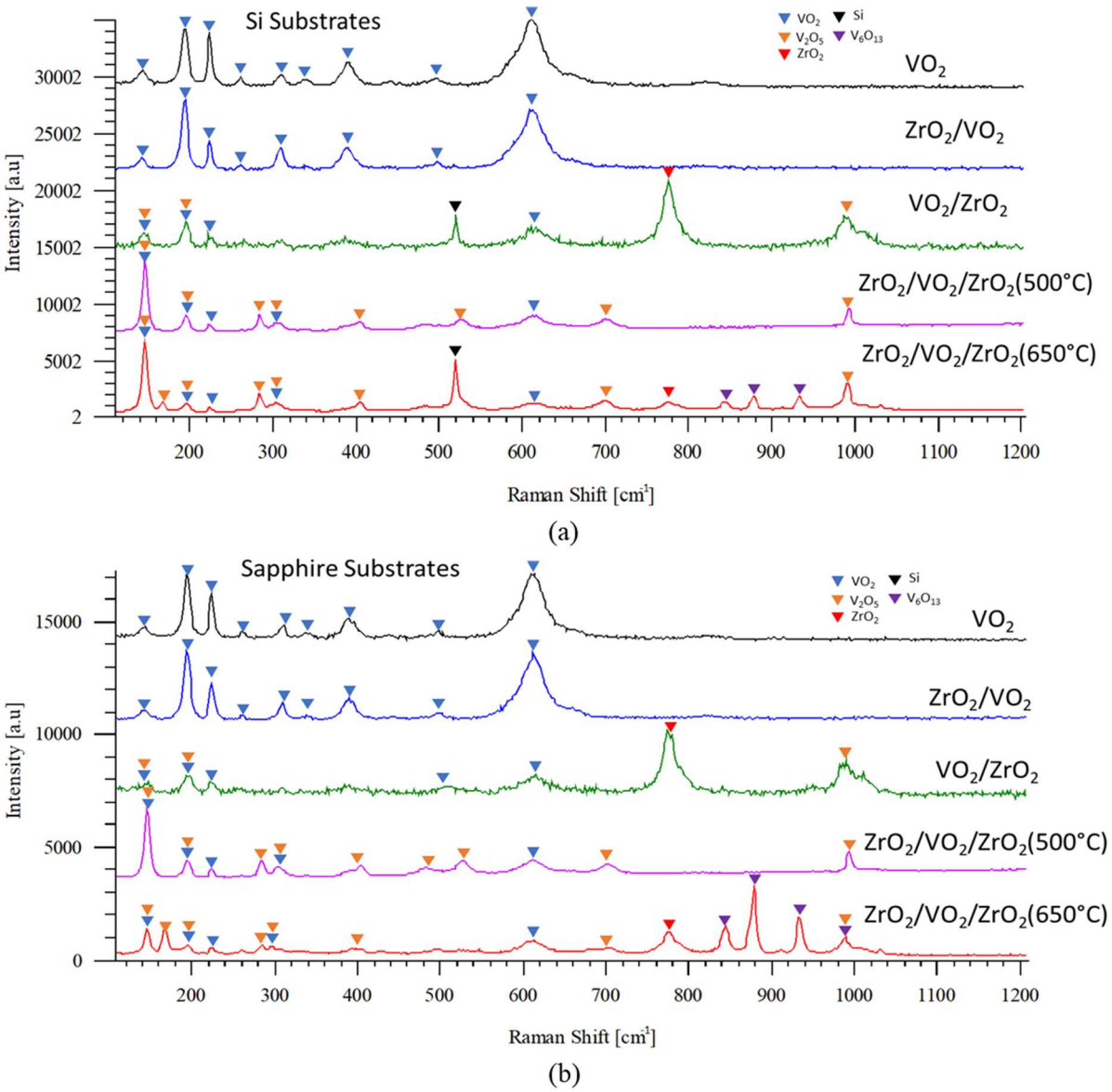

Figure 4.1: Raman spectra of samples on Si (a) and sapphire (b) substrates

4.1.2 Surface roughness

Surface roughness has well known effects on optical properties of thin films. This is primarily due to changes in scattering at the surfaces with changing roughness. Increasing roughness leads to increased scattering and decreased transmittance through a given film. Changes due to increased scattering can also heavily affect interference film designs which require precise control of light interactions. As this is a common use for multilayer designs in applications such

as smart radiators, and optical switches, roughness is an important feature of thin films to be considered.

A summary of roughness values of the prepared films is presented in table 4.1. All samples show relatively low roughness values, ranging between 1.0 nm and 11.6 nm. Single-layer VO_2 and ZrO_2/VO_2 films show lower roughness values compared to the samples with ZrO_2 as a top layer. Bi-layered VO_2/ZrO_2 samples and $ZrO_2/VO_2/ZrO_2$(650 °C) samples both show higher roughness than $ZrO_2/VO_2/ZrO_2$(500 °C) samples. This agrees well with the Raman results which indicate that the top ZrO_2 layer in the $ZrO_2/VO_2/ZrO_2$(500 °C) samples is amorphous (it is reasonable that amorphous ZrO_2 in the $ZrO_2/VO_2/ZrO_2$(500 °C) samples has lower roughness than crystalline ZrO_2 in the $ZrO_2/VO_2/ZrO_2$(650 °C) samples). Nevertheless, the $ZrO_2/VO_2/ZrO_2$(500 °C) films have higher roughness values than the samples with crystalline VO_2 top layer. This indicates that during the deposition of the top ZrO_2 layer, the VO_2 underlayer went through grain growth and phase transition as displayed in the SEM images shown in section 4.1.3.

Table 4.1: Roughness values of thermochromic thin film samples on Si substrates

Sample	Si sample RMS Roughness (nm)
VO_2	1.8±0.4
ZrO_2/VO_2	2.2±0.4
VO_2/ZrO_2	7.0±0.7
$ZrO_2/VO_2/ZrO_2$(500 °C)	3.0±0
$ZrO_2/VO_2/ZrO_2$(650 °C)	5.2±0.4

4.1.3 SEM Imaging

Figures 4.2a-e show the cross-section images of Samples deposited on Si wafers. The image shown in figure 4.8a displays a single VO_2 layer of 334±16 nm. Figure 4.2b shows that the ZrO_2/VO_2 bi-layer sample has a VO_2 layer of 297±13 nm and a ZrO_2 layer of 116±3 nm. The ZrO_2 layer in those samples shows smaller crystallite size compared to the VO_2 layer.

The image shown in figure 4.2c displays three distinct layers, a top layer of 88±9 nm, a middle layer of 216±11 nm, and a bottom layer of 145±17 nm. The top layer being ZrO_2 and the bottom two layers being V_2O_5 and VO_2 as both of these vanadium oxides were shown in Raman testing. These areas are highlighted in figure 4.3a. It is more likely that the middle layer of this sample is

V_2O_5, as the top of this layer was exposed to the environment with oxygen during the ZrO_2 deposition process. Another possibility is that the middle layer consists of mixed phase structure containing both VO_2 and V_2O_5.

This similar pattern with an extra layer between top and bottom ZrO_2 layers can be seen in triple-layered samples deposited at 650 °C, as shown in figure 4.2e and figure 4.3c with layers labeled. In this sample, the thickness of the top ZrO_2 layer and bottom ZrO_2 layer are 77±5 nm and 95±8 nm, respectively. The middle V-O layer is of 429±10 nm thick, which includes a bottom layer of 301±9 nm and the upper layer of 128±10 nm. The triple-layered samples with a top layer deposited at a temperature of 500 °C do not show a clear separation in the middle V_xO_y layer which is 273±13 nm thick. This sample shows a top ZrO_2 layer of 59±4 nm and a 86±6 nm thick bottom ZrO_2 layer.

Previous research shows that the layer thickness has less impact than crystalline quality on the transmittance of optical thin film transmittance [129] [130]. Samples with crystal structure of similar high quality but different thicknesses have been shown to have similar overall transmittance. For VO_2 films, Yang et al. [131] showed less prevalent changes in hysteresis properties than what was observed in section 4.2.2 of this work. This suggests that the variations in thickness of the deposited layers are not as significant as the change of layer structures and the resulting structural changes.

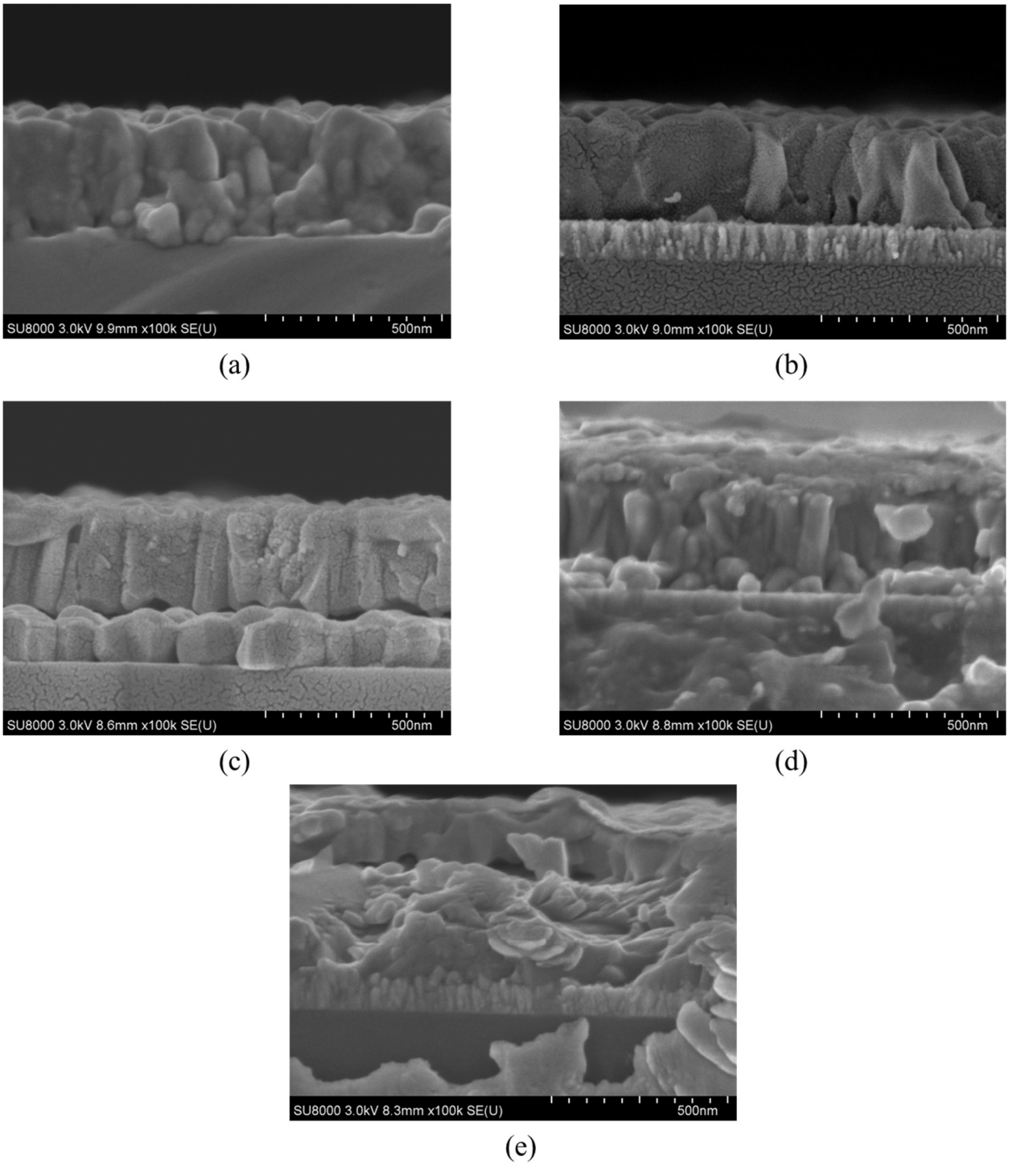

Figure 4.2: SEM cross-section images of Single layer VO_2 (a), ZrO_2/VO_2 (b), VO_2/ZrO_2 (c), $ZrO_2/VO_2/ZrO_2$(500°C) (d), and $ZrO_2/VO_2/ZrO_2$(650°C) (e) samples on Si substrates

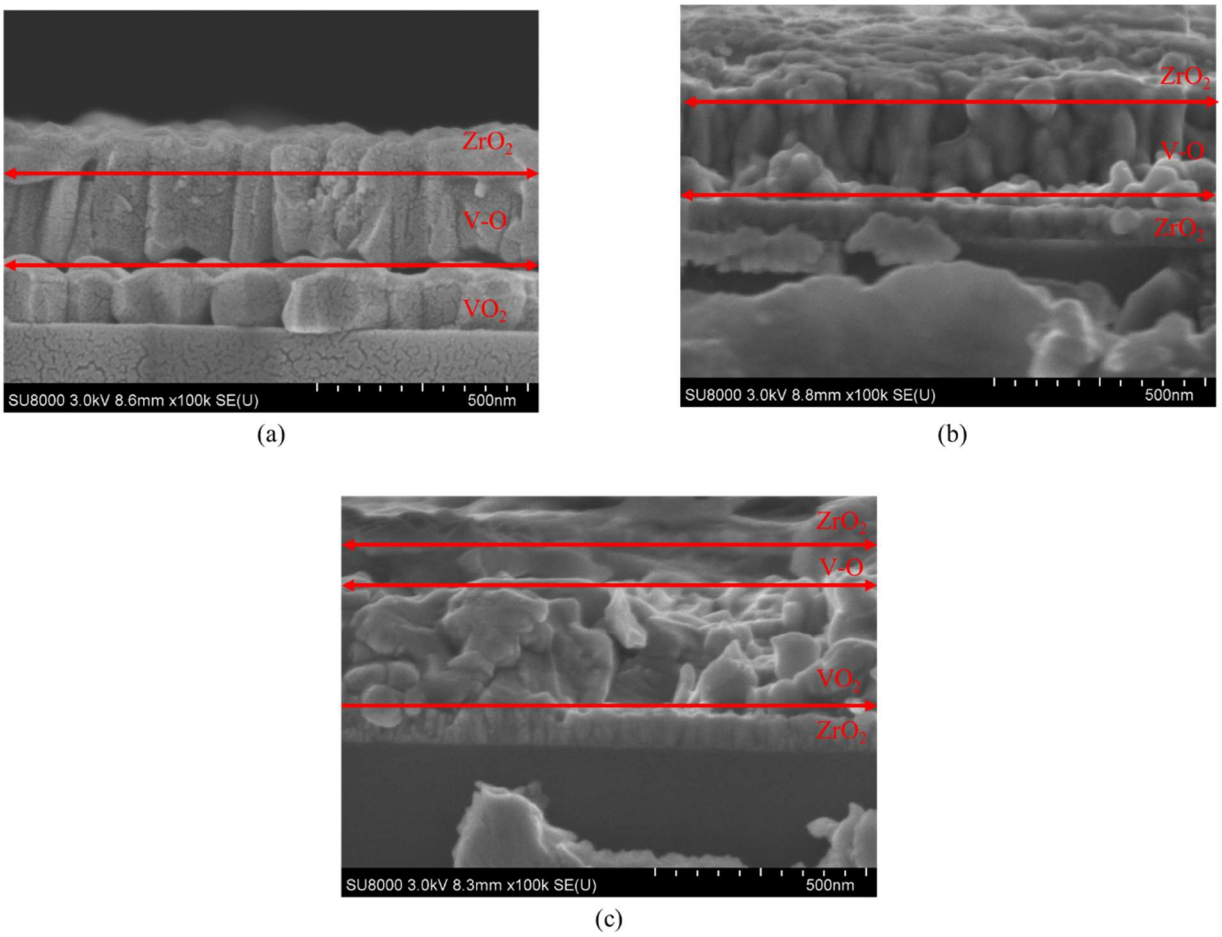

Figure 4.3: SEM images of bi-layer VO_2/ZrO_2 (a), $ZrO_2/VO_2/ZrO_2$(500°C) (b), and $ZrO_2/VO_2/ZrO_2$(650°C) (c) films with layers labeled

Structural studies presented so far in this study suggest that the increased oxygen content and high temperature used to deposit ZrO_2 on top of the VO_2 layer leads to unwanted changes in structure and oxidation of the VO_2 layer. ZrO_2, however, does not show significant structural change when used as a buffer layer between the substrate and the VO_2 layer. Because of this, VO_2 is preferred to be the top layer for high quality multilayered thin film device designs. If a given device design requires the use of VO_2 as an internal layer, the top oxide layer should be able to be deposited at low oxygen pressure and low temperature to prevent the VO_2 layer from oxidization. As crystalline ZrO_2 as a top layer cannot be obtained at a temperature of 500 °C, ZrO_2 is not suitable to be a top layer in making VO_2 thin film based devices with the reactive magnetron sputtering method.

4.2 Optical characteristics of VO_2 based thermochromic thin films

4.2.1 Transmittance

Transmittance spectra of the samples in their insulating (room temperature) and metallic state (elevated temperature) are shown in figures 4.4 – 4.7. Figure 4.4 shows the transmittance of single layered VO_2 samples on Si (a) and Sapphire (b) substrates. The transmittance of both samples in the insulating and metallic states agrees well with that reported previously for single-layered VO_2 samples [132], [133].

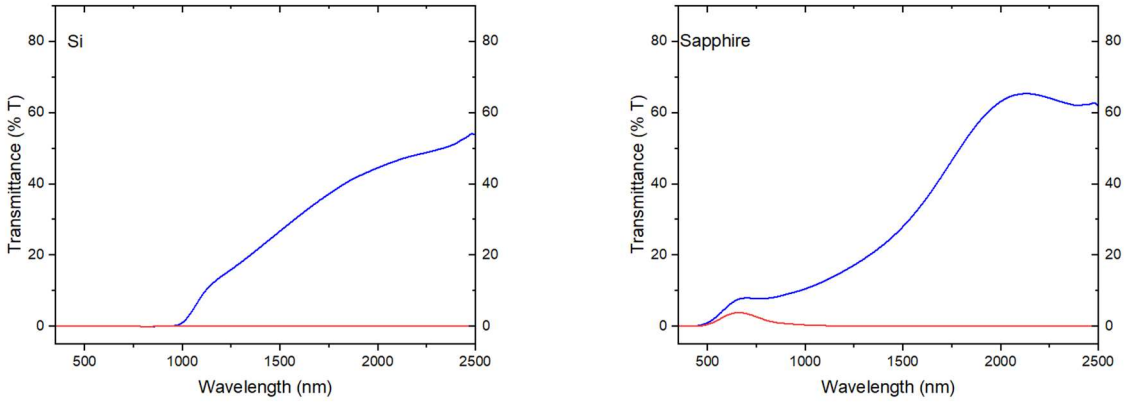

Figure 4.4: Transmittance in insulating and metallic states of single-layered VO_2 on Si (a) and Sapphire (b) substrates.

Figure 4.5 shows the transmittance spectra of ZrO_2/VO_2 samples on Si (a) and sapphire (b) substrates. It can be seen that the addition of a ZrO_2 bottom layer increases the transmittance of samples on Si from 1600 nm to 2000 nm and the transmittance of samples on sapphire consistently from 700 am to 2500 nm. Both samples show near zero transmittance in their metallic state. A previous study has shown increased transmittance of VO_2 thin films both at an insulating and metallic state when ZrO_2 was added as a bottom layer using PLD on glass substrates [134]. Increased transmittance for single-layered VO_2 films has been related to improved crystalline quality and decreased defects [40], [135]. This suggests that the bottom ZrO_2 may improve these qualities of the VO_2 layer in these bi-layered samples.

Figure 4.6 shows the transmittance spectra of VO_2/ZrO_2 films. Both samples show decreased transmittance at insulating state, and certain degree of transmittance (non-opaque) over the measured wavelengths after transition to metallic state. This is likely due to the partial oxidization of VO_2 into V_2O_5 when depositing ZrO_2 on it at a high temperature of 650 °C. Previous studies have shown that thin film samples with mixed phases of $VO_2 + V_2O_5$ were non-opaque after phase transition to metallic state [40].

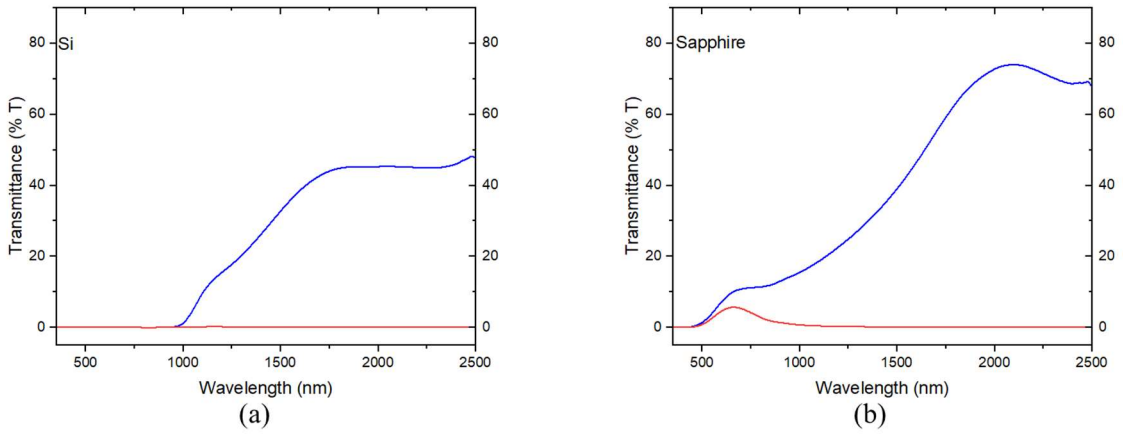

Figure 4.5: Transmittance in insulating (blue) and metallic (red) states for ZrO_2/VO_2 Si (a) and Sapphire (b) substrates

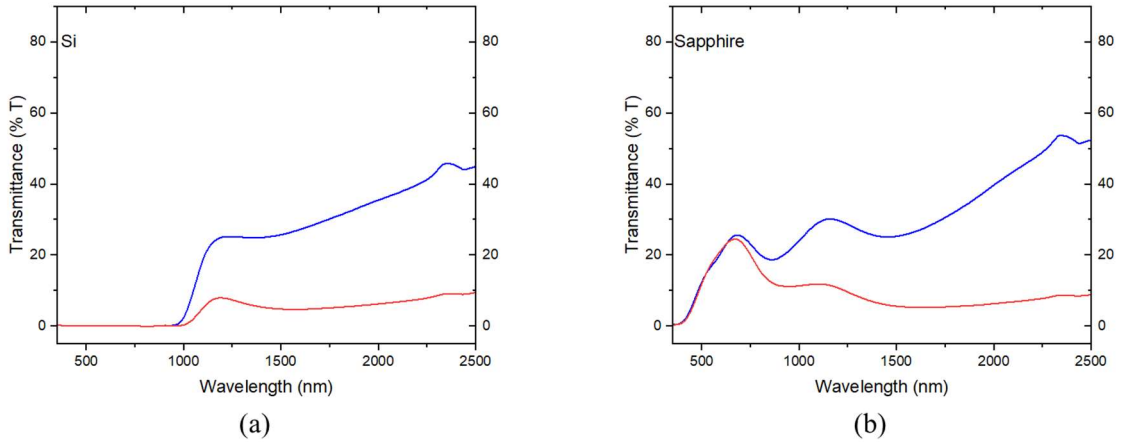

Figure 4.6: Transmittance in insulating (blue) and metallic states (red) of VO_2/ZrO_2 on Si (a) and Sapphire (b) substrates

Figure 4.7 shows the transmittance of triple-layered samples with a top layer deposited at 500 °C and 650 °C on Si and sapphire substrates. The $ZrO_2/VO_2/ZrO_2$(500 °C) samples show increased transmittance before transition and a near-zero transmittance after transition. This suggests that mixed phased VO_2 samples can be opaque if the oxidation is limited. With the top layer deposited at 650 °C, there is a slight decrease in transmittance before transition and certain degree of transmittance after transition. Similar to the VO_2/ZrO_2 sample this is likely due to the presence of additional vanadium oxides formed during the deposition of top ZrO_2 layer at 650 °C.

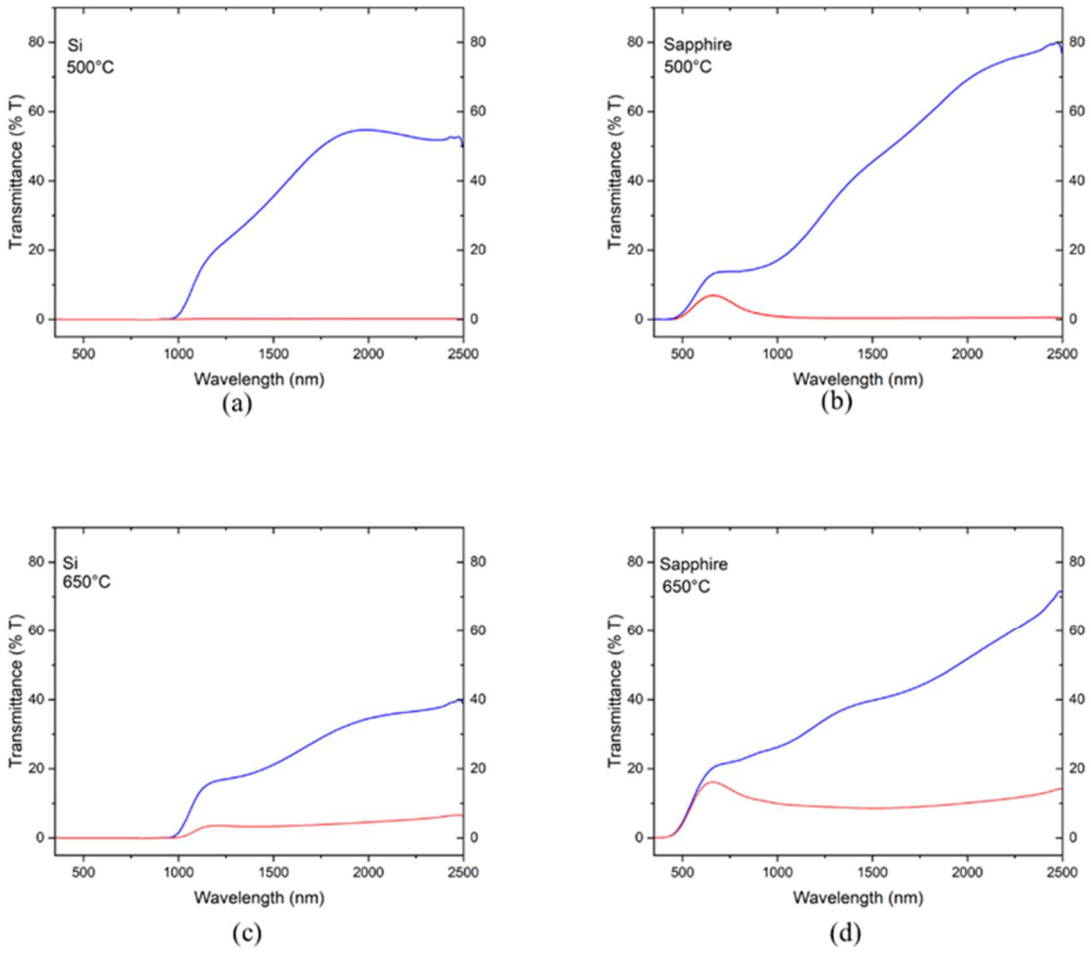

Figure 4.7: Transmittance in insulating (blue) and metallic states (red) of $ZrO_2/VO_2/ZrO_2$(500 °C) (a,b) and $ZrO_2/VO_2/ZrO_2$(650 °C) (c,d) samples

For smart window applications, common performance metrics are the luminous and solar transmittance efficiency or T_{lum} and T_{sol}, respectively [14], [15], [79], [136]. For the samples prepared on sapphire substrates in this study, these factors are calculated based on the transmittance spectra shown in Figs 11-13 utilizing equation 4.1 adapted from Zhang et al. [135] and are summarized in table 4.2. In equation 4.1, $\varphi_{lum,sol}$ describes the modification factors for T_{lum} and T_{sol} calculations. These factors are multiplied by the transmittance values of a film at their respective wavelengths before being summed over the relevant spectrum. This is then divided by the unaltered transmittance summation over the same wavelength range. This gives values of T_{lum} and T_{sol} in percentage values.

Luminous efficiency describes how well people can see light in a given spectrum and relates to the wavelengths between 380 – 780 nm modified by the spectral luminous efficiency function [137]. Minimizing the decrease in T_{lum} following the IMT is desired as this will lead to less vision loss in spaces utilizing a given film for smart window applications.

Solar Transmittance efficiency (T_{sol}) is a value which describes the summation of the solar transmittance in the near infrared spectrum (250 – 2500 nm) and is modified by the ASTM G-137 extraterrestrial radiation spectrum [138]. For smart window VO_2 applications, it is desirable to have a significant decrease in T_{sol} through the IMT transition, which will lead to more effective heating reduction spaces using smart window coatings.

$$T_{lum,sol} = \frac{\int \varphi_{lum,sol}(\lambda) T(\lambda) d\lambda}{\int \varphi_{lum,sol}(\lambda) d\lambda} \tag{4.1}$$

Table 4.2: luminous and solar efficiencies for thermochromic films prepared on sapphire substrates

Sample Structure	T_{lum}(%) (Insulating State)	T_{lum}(%) (Metallic State)	ΔT_{lum}(%)	T_{sol}(%) (Insulating State)	T_{sol}(%) (Metallic State)	ΔT_{sol}(%)
VO_2	3.4	1.9	1.5	11.4	1.1	10.3
ZrO_2/VO_2	4.5	2.9	1.6	15.1	1.7	13.4

VO_2/ZrO_2	17.4	18	-0.6	19.9	12.2	7.7
$ZrO_2/VO_2/ZrO_2$(500°C)	6.4	3.8	2.6	17.3	2.2	15.1
$ZrO_2/VO_2/ZrO_2$(650°C)	11.6	10.5	1.1	20.4	9.1	11.4

Single-layer VO_2 and ZrO_2/VO_2 samples show the lowest insulating state T_{lum} values. This indicates that even prior to the IMT transition there would be possible issues with indoor vision. The VO_2/ZrO_2 shows the highest T_{lum} value prior to the transition for all the samples studied, and a small increase of T_{lum} after transition. This coupled with the large change in T_{sol} values during the IMT has demonstrated that ZrO_2/VO_2 films are promising for smart window applications. For triple-layer films, the increased top layer deposition temperature leads to slightly decreased solar modulation, but a more reasonable luminous efficiency before and after the transition. A further consideration for use in smart windows is the IMT transition temperature. As noted in chapter 2.4.1, it is generally desired to reduce the T_{IMT} of pure VO_2 from 69 °C. The samples that show promise as smart windows all show increased transition temperatures. To effectively use these films in smart window applications, some additional modifications such as elemental doping would be required to reduce the T_{IMT}.

4.2.2 Hysteresis

To determine the effect of layer structures on the phase transition properties, hysteresis testing was done by measuring the transmittance of samples at the 1550 nm wavelength over the IMT and MIT for samples which occur during the heating and cooling steps, respectively. This data is first presented as transmittance % related to temperature in figures 4.9 and 4.10. To further quantify transition, the hysteresis data is presented in $|(d\tilde{T})/dT|$ vs. temperature plots in figures 4.10 – 4.14. This is a common method used to give more quantifiable values to describe transition properties of VO_2 based films. Figure 4.8 shows single-layer VO_2 hysteresis results on Si substrate in the transmittance % vs. temperature (a) and the $|(d\tilde{T})/dT|$ vs. temperature (b) with important features noted.

In figure 4.8a, the hysteresis testing steps of heating and cooling are noted. The sharpness of the transition can be qualitatively seen in figure 4.9a as the range of temperatures between the

beginning and end of significant changes in transmittance values. This is quantitatively described in figure 4.8b as full width half maximum (FWHM) values, with a lower value corresponding to a sharper transition step. The initiation of the phase transition is shown in figure 4.8b as the T_{IMT} and T_{MIT} values, which correspond with the point of highest slope in heating and cooling curves in figure 4.8a respectively. The hysteresis width highlighted in figure 4.8a corresponds with the ΔH values shown in figure 4.9b and is calculated by the difference between T_{IMT} and T_{MIT} values. The discussion in this section will be focused on figures 4.11 – 4.14 while figures 4.9 and 4.10 will serve as a reference to actual transmittance through samples at 1550 nm.

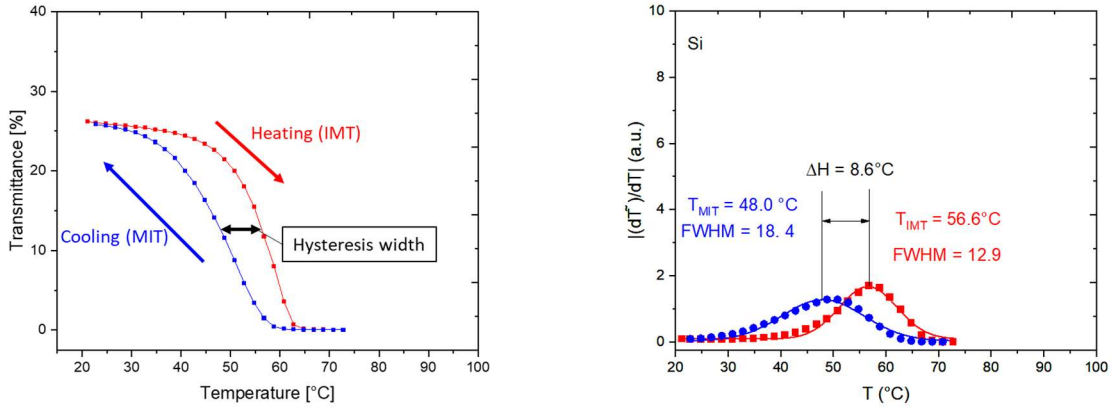

Figure 4.8: Single-layer VO2 on Si sample hysteresis testing as transmittance % vs. temperature (a) and $|(d\tilde{T})/dT|$ vs. temperature (b)

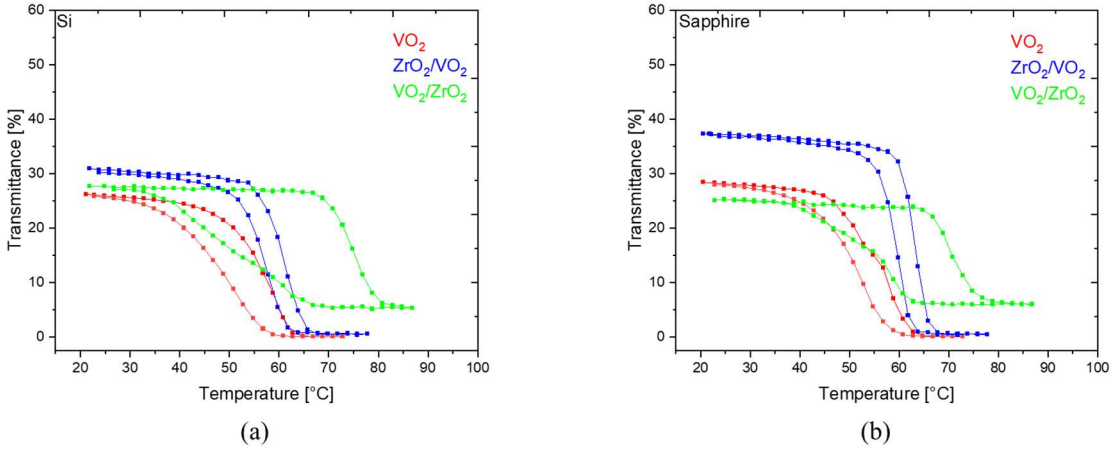

Figure 4.9: Hysteresis testing results of bi-layer samples and single-layer VO_2 samples on Si (a) and sapphire (b) at 1550 nm wavelength

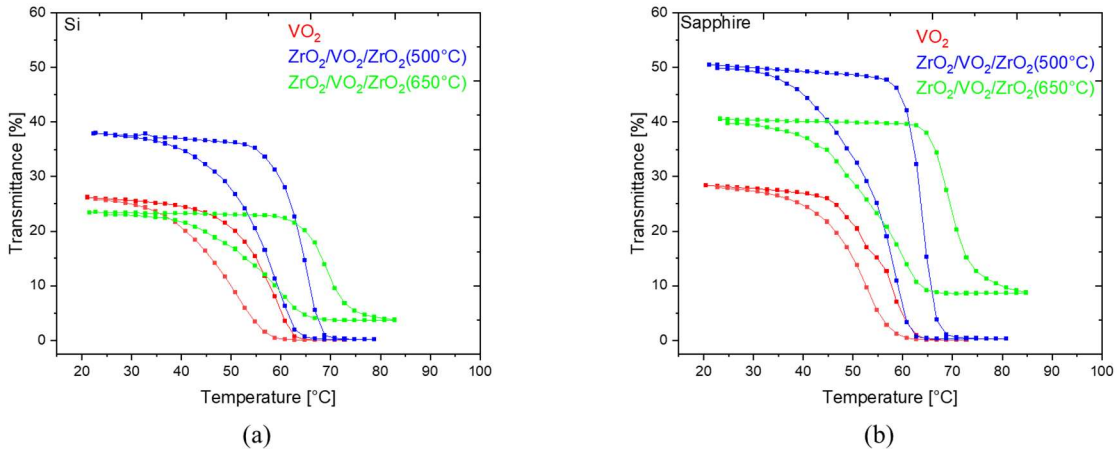

Figure 4.10: Hysteresis testing results of triple-layer samples and single-layer VO_2 on Si (a) and sapphire (b) at 1550 nm wavelength

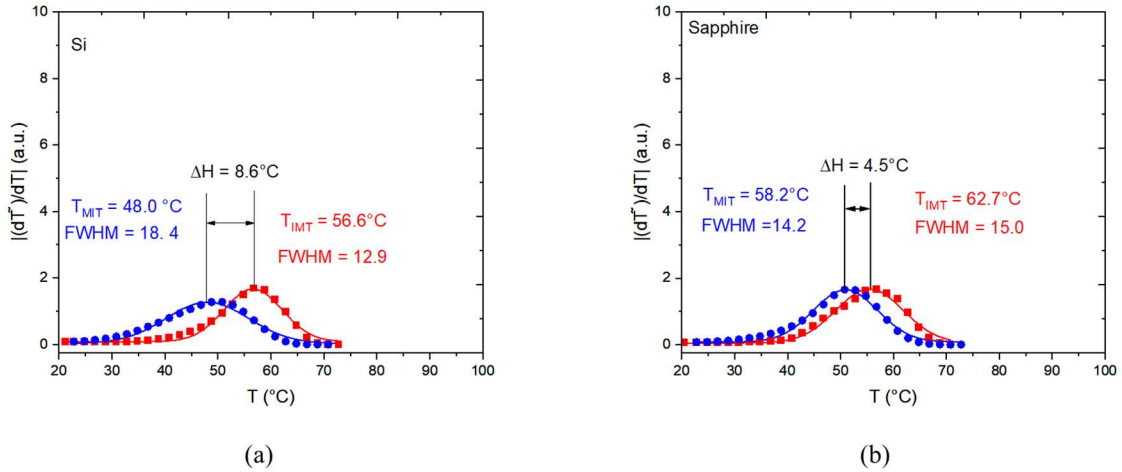

Figure 4.11: Temperature dependence on transition properties of VO2 films on Si (a) and sapphire (b) substrates

Figure 4.11 shows hysteresis properties of single-layer VO_2 samples on Si (a) and sapphire (b). These results will be used as references to understand the changes caused by the changing layer structures. For both substrates in figure 4.17 (a) and (b) ZrO_2/VO_2 samples show a sharp transition with FWHM ranging between 5.9 and 8.1 and low ΔH values of 3.8 for both Si and sapphire samples, indicating a higher degree of VO_2 crystallization. These samples also show similar T_{IMT} values when compared to single-layer samples.

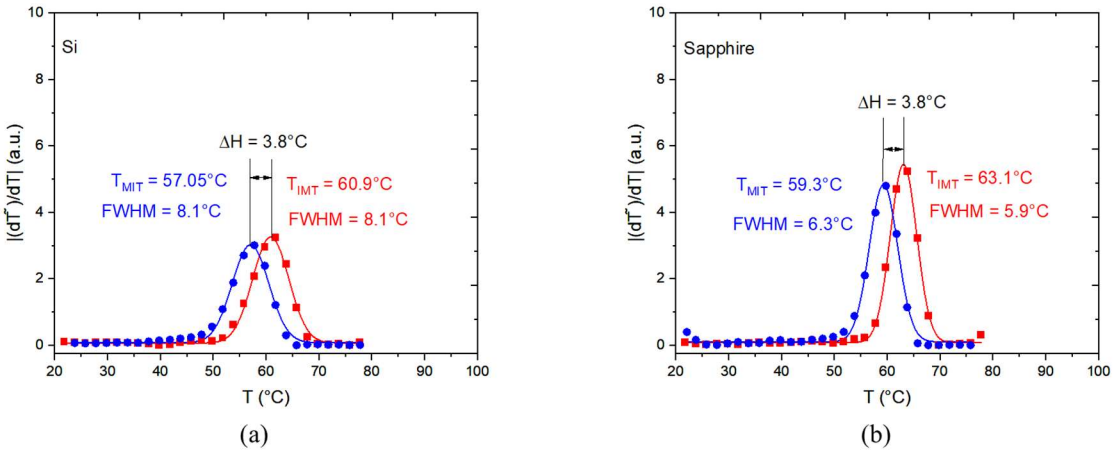

Figure 4.12: Temperature dependence on transition properties of ZrO_2/VO_2 films on Si (a) and sapphire (b) substrates

VO_2/ZrO_2 samples seen in figure 4.13 show the largest hysteresis width with the highest T_{IMT} of all samples prepared. This is likely due to an increase in oxidation of the VO_2 phase, as it has been seen in previous research [125]. $FWHM_{IMT}$ values for VO_2/ZrO_2 samples on Si and sapphire substrates show a decrease compared to single-layer VO_2. These samples also show significant increases ΔH values of 30.7 °C and 17.9 °C on Si and sapphire substrates respectively.

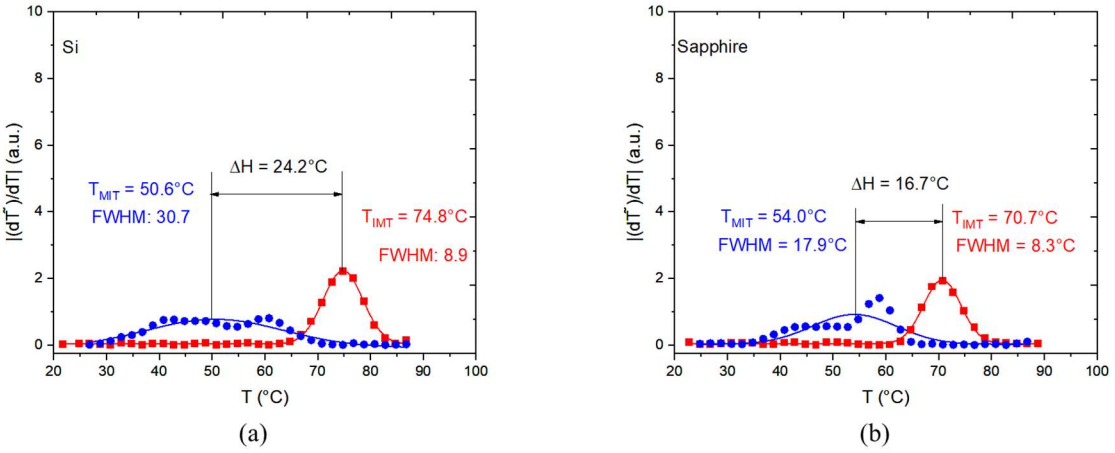

Figure 4.13: Temperature dependence on transition properties of VO_2/ZrO_2 films on Si (a) and sapphire (b) substrates

Figure 4.14 shows the hysteresis characteristics of samples on Si and Sapphire for triple-layered samples with top layer depositions of 500 °C and 650 °C respectively. For all triple-layered

samples, there is an increase in T_{IMT}. In all samples with the exception of the 500 °C sample on Si, ΔH values are increased compared to single-layer VO_2. The 650 °C samples show the higher increase in both T_{IMT} and ΔH. It is likely that the increase in hysteresis width and T_{IMT} are from the increasing oxidation of triple-layered samples deposited at 650 °C. All triple-layer samples also show much smaller $FWHM_{IMT}$ values than $FWHM_{MIT}$.

For VO_2/ZrO_2 and triple-layer samples, there is a pattern of increased T_{IMT} values and increased hysteresis width. There is also a pattern of increased sharpness in the insulator-metal transition when compared to the metal-insulator transition for these samples ($FWHM_{IMT}$ being smaller than $FWHM_{MIT}$). All of these samples also showed oxidation of the VO_2 layer due to the top layer deposition of ZrO_2. This indicates that this oxidation is a likely cause for these hysteresis patterns.

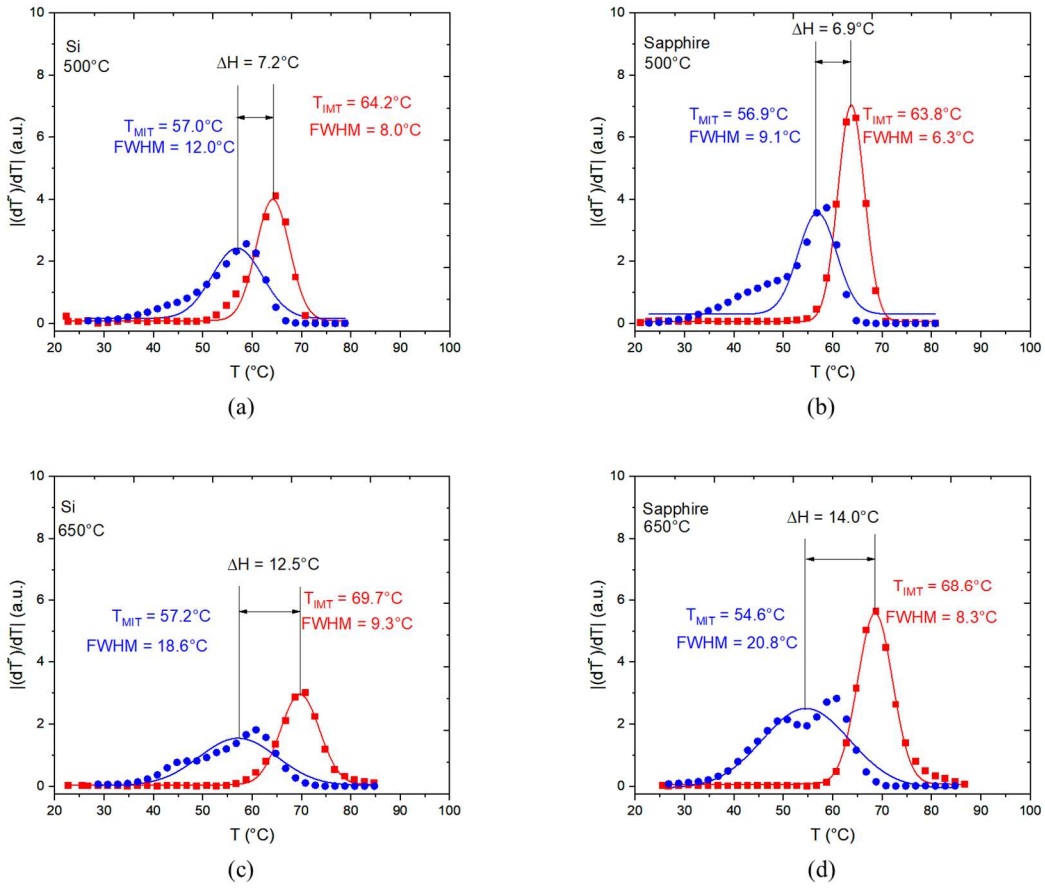

Figure 4.14: Temperature dependence on transition properties of $ZrO_2/VO_2/ZrO_2$(500 °C) (a,b) and $ZrO_2/VO_2/ZrO_2$(650 °C) (c,d) samples

CHAPTER 5 – CONCLUSIONS AND FUTURE WORK RECOMMENDATIONS

5.1 Summary and Conclusions

Thermochromic VO_2+ZrO_2 based films with three distinct layer structures have been synthesized using reactive magnetron sputtering techniques. Specifically, the layer structures include bi-layer films with ZrO_2 deposited below and above VO_2 layers and triple-layers with ZrO_2 above and below a VO_2 middle layer. The effects of these layer structures on the structural, optical, and thermochromic transition properties of VO_2 films have been studied and are detailed below:

1. The deposition of ZrO_2 film on a VO_2 layer at high temperature and high oxygen partial pressure has been shown to form V_2O_5 and V_6O_{13} from the VO_2 layer, leading to widened hysteresis and higher IMT transition temperatures.
2. Bi-layer films with ZrO_2 as a bottom layer show high transmittance and a sharp transition to opaqueness, both characteristics that hold promise for optical switching applications.
3. ZrO_2 shows sufficient thermal stability to maintain a crystalline structure when used as a base layer in multilayer films.
4. Films with V_2O_5 and V_6O_{13} present have lower ΔT_{lum} (%) in combinations with higher ΔT_{sol} (%), showing promise for smart window applications if combined with further modifications that lower the T_{IMT}.

5.2 Future Recommendations

This study has shown that the addition of ZrO_2 layers modified the thermochromic properties of VO_2 thin films, demonstrating promising properties for optical switch and smart widow application. Further research in applications of these thin films is suggested as follows.

1. Use the high performing ZrO_2/VO_2 structure as the top layers of more complex layered designs including well studied optical bandpass or line pass filters. Study of these designs would combine phase switching and light filtering that can be used for unique optical switching applications.

2. Since VO_2/ZrO_2 bi-layer samples showed promise for smart window applications, a further study into these coatings for smart windows should be done. This would include preparation of VO_2/ZrO_2 samples on different glass substrates, testing of their optical/phase transition properties. Since these samples show high T_{IMT}, to be effective in smart coatings, doping of the Vanadium oxide layer with elements such as W, and Al may be necessary. If this proves successful in lowering the T_{IMT}, small-scale testing of these samples on internal building temperatures may be warranted.
3. Synthesize and test structural and optical properties of multilayered thin films with different oxides, specifically, ones that have shown promise in past research and have compatible refractive indices such as ZnO, WO_3, and TiO_2.

References

[1] "Government of Canada announces significant investment in the Canadian semiconductor and photonics industries - Canada.ca." Accessed: Jan. 04, 2024. [Online]. Available: https://www.canada.ca/en/innovation-science-economic-development/news/2022/02/government-of-canada-announces-significant-investment-in-the-canadian-semiconductor-and-photonics-industries.html

[2] "FACT SHEET: CHIPS and Science Act Will Lower Costs, Create Jobs, Strengthen Supply Chains, and Counter China | The White House." Accessed: Jan. 04, 2024. [Online]. Available: https://www.whitehouse.gov/briefing-room/statements-releases/2022/08/09/fact-sheet-chips-and-science-act-will-lower-costs-create-jobs-strengthen-supply-chains-and-counter-china/

[3] F. J. Morin, "Oxides Which Show a Metal-to-Insulator Transition at the Neel Temperature," Phys Rev Lett, vol. 3, no. 1, 1959.

[4] J. Yoon, W. K. Hong, Y. Kim, and S. Y. Park, "Nanostructured Vanadium Dioxide Materials for Optical Sensing Applications," Sensors 2023, Vol. 23, Page 6715, vol. 23, no. 15, p. 6715, Jul. 2023, doi: 10.3390/S23156715.

[5] J. Yoon, W. K. Hong, Y. Kim, and S. Y. Park, "Nanostructured Vanadium Dioxide Materials for Optical Sensing Applications," Sensors 2023, Vol. 23, Page 6715, vol. 23, no. 15, p. 6715, Jul. 2023, doi: 10.3390/S23156715.

[6] J. Zha et al., "Infrared Photodetectors Based on 2D Materials and Nanophotonics," Adv Funct Mater, vol. 32, no. 15, p. 2111970, Apr. 2022, doi: 10.1002/ADFM.202111970.

[7] S. Song et al., "Tailoring active color rendering and multiband photodetection in a vanadium-dioxide-based metamaterial absorber," Photonics Research, Vol. 6, Issue 6, pp. 492-497, vol. 6, no. 6, pp. 492–497, Jun. 2018, doi: 10.1364/PRJ.6.000492.

[8] S. Balendhran et al., "Flexible Vanadium Dioxide Photodetectors for Visible to Longwave Infrared Detection at Room Temperature," Adv Funct Mater, vol. 33, no. 42, p. 2301790, Oct. 2023, doi: 10.1002/ADFM.202301790.

[9] S. Chen et al., "Optical switch based on vanadium dioxide thin films," Infrared Phys Technol, vol. 45, no. 4, pp. 239–242, Jul. 2004, doi: 10.1016/J.INFRARED.2003.11.005.

[10] H. Kim et al., "Flexible thermochromic window based on hybridized VO2/graphene," ACS Nano, vol. 7, no. 7, pp. 5769–5776, Jul. 2013, doi: 10.1021/NN400358X/SUPPL_FILE/NN400358X_SI_001.PDF.

[11] J. Outón, A. Casas-Acuña, M. Domínguez, E. Blanco, J. J. Delgado, and M. Ramírez-del-Solar, "Novel laser texturing of W-doped VO2 thin film for the improvement of luminous transmittance

in smart windows application," Appl Surf Sci, vol. 608, p. 155180, Jan. 2023, doi: 10.1016/J.APSUSC.2022.155180.

[12] J. Wu et al., "Facile Synthesis of Island-like ZrO2-VO2 Composite Films with Enhanced Thermochromic Performance for Smart Windows," Materials 2023, Vol. 16, Page 273, vol. 16, no. 1, p. 273, Dec. 2022, doi: 10.3390/MA16010273.

[13] N. Suzuki, Y. Xue, T. Hasegawa, and S. Yin, "Phase transition behavior and optical properties of F/Mo co-doped VO2 for smart windows," Solar Energy Materials and Solar Cells, vol. 251, p. 112105, Mar. 2023, doi: 10.1016/J.SOLMAT.2022.112105.

[14] K. Okimura, M. S. Mian, I. Yamaguchi, and T. Tsuchiya, "High luminous transmittance and solar modulation of VO2-based smart windows with SiO2 anti-reflection coatings," Solar Energy Materials and Solar Cells, vol. 251, p. 112162, Mar. 2023, doi: 10.1016/J.SOLMAT.2022.112162.

[15] T. Chang et al., "Optical design and stability study for ultrahigh-performance and long-lived vanadium dioxide-based thermochromic coatings," Nano Energy, vol. 44, pp. 256–264, Feb. 2018, doi: 10.1016/J.NANOEN.2017.11.061.

[16] M. Saeli, C. Piccirillo, I. P. Parkin, I. Ridley, and R. Binions, "Nano-composite thermochromic thin films and their application in energy-efficient glazing," Solar Energy Materials and Solar Cells, vol. 94, no. 2, pp. 141–151, Feb. 2010, doi: 10.1016/J.SOLMAT.2009.08.010.

[17] J. Liang et al., "Room temperature H2S gas sensing performance of VO2(A) nanowires with high aspect ratio," Sens Actuators A Phys, vol. 347, p. 113986, Nov. 2022, doi: 10.1016/J.SNA.2022.113986.

[18] X. Xu, R. Xu, and Y. S. Lin, "A voltage-controllable VO2 based metamaterial perfect absorber for CO2 gas sensing application," Nanoscale, vol. 14, no. 7, pp. 2722–2728, Feb. 2022, doi: 10.1039/D1NR07746E.

[19] L. Lin, R. Chen, J. Huang, P. Wang, H. Tao, and Z. Zhang, "Adsorption of gas molecules of CH4, CO and H2O on the vanadium dioxide monolayer: computational method and model," Journal of Physics: Condensed Matter, vol. 33, no. 5, p. 055502, Nov. 2020, doi: 10.1088/1361-648X/ABBCFA.

[20] A. Hendaoui, N. Émond, S. Dorval, M. Chaker, and E. Haddad, "Enhancement of the positive emittance-switching performance of thermochromic VO2 films deposited on Al substrate for an efficient passive thermal control of spacecrafts," Current Applied Physics, vol. 13, no. 5, pp. 875–879, Jul. 2013, doi: 10.1016/J.CAP.2012.12.028.

[21] A. Hendaoui, N. Émond, M. Chaker, and É. Haddad, "Highly tunable-emittance radiator based on semiconductor-metal transition of VO2 thin films," Appl Phys Lett, vol. 102, no. 6, p. 61107, Feb. 2013, doi: 10.1063/1.4792277/26111.

[22] A. Hendaoui, N. Émond, S. Dorval, M. Chaker, and E. Haddad, “VO2-based smart coatings with improved emittance-switching properties for an energy-efficient near room-temperature thermal control of spacecrafts,” Solar Energy Materials and Solar Cells, vol. 117, pp. 494–498, Oct. 2013, doi: 10.1016/J.SOLMAT.2013.07.023.

[23] S. Taylor, Y. Yang, and L. Wang, “Vanadium dioxide based Fabry-Perot emitter for dynamic radiative cooling applications,” J Quant Spectrosc Radiat Transf, vol. 197, pp. 76–83, Aug. 2017, doi: 10.1016/J.JQSRT.2017.01.014.

[24] H. A. Wriedt, “The O-V (Oxygen-Vanadium) system,” Bulletin of Alloy Phase Diagrams, vol. 10, no. 3, pp. 271–277, Jun. 1989, doi: 10.1007/BF02877512/METRICS.

[25] M. H. Lee, Y. Kalcheim, J. Del Valle, and I. K. Schuller, “Controlling Metal-Insulator Transitions in Vanadium Oxide Thin Films by Modifying Oxygen Stoichiometry,” ACS Appl Mater Interfaces, vol. 13, no. 1, pp. 887–896, Jan. 2021, doi: 10.1021/ACSAMI.0C18327/ASSET/IMAGES/LARGE/AM0C18327_0008.JPEG.

[26] C. Zhang, O. Gunes, S. J. Wen, Q. Yang, and S. Kasap, “Effect of Substrate Temperature on the Structural, Optical and Electrical Properties of DC Magnetron Sputtered VO2 Thin Films,” Materials 2022, Vol. 15, Page 7849, vol. 15, no. 21, p. 7849, Nov. 2022, doi: 10.3390/MA15217849.

[27] C. Zhang et al., “Characterization of vanadium oxide thin films with different stoichiometry using Raman spectroscopy,” Thin Solid Films, vol. 620, pp. 64–69, Dec. 2016, doi: 10.1016/J.TSF.2016.07.082.

[28] B. Rajeswaran and A. M. Umarji, “Comparing the effect of synthesis techniques on the semiconductor-metal transition of VO2 thin films,” Mater Lett, vol. 339, p. 134108, May 2023, doi: 10.1016/J.MATLET.2023.134108.

[29] Z. Shao, X. Cao, H. Luo, and P. Jin, “Recent progress in the phase-transition mechanism and modulation of vanadium dioxide materials,” NPG Asia Materials 2018 10:7, vol. 10, no. 7, pp. 581–605, Jul. 2018, doi: 10.1038/s41427-018-0061-2.

[30] M. Eaton, A. Catellani, and A. Calzolari, “VO2 as a natural optical metamaterial,” Optics Express, Vol. 26, Issue 5, pp. 5342-5357, vol. 26, no. 5, pp. 5342–5357, Mar. 2018, doi: 10.1364/OE.26.005342.

[31] Rudolf E. Peierls, More Surprises in Theroretical Physics. Princeton University Press , 1991.

[32] A. Zylbersztejn and N. F. Mott, “Metal-insulator transition in vanadium dioxide*,” 1975.

[33] R. M. Wentzcovitch, W. W. Schulz~, and P. B. Allen, “VO2’. Peierls or Mott-Hubbard? A View from Band Theory,” vol. 72, 1994.

[34] J. B. Goodenough, “The two components of the crystallographic transition in VO2,” J Solid State Chem, vol. 3, no. 4, pp. 490–500, Nov. 1971, doi: 10.1016/0022-4596(71)90091-0.

[35] D. Lee et al., “Deposition-Temperature-Mediated Selective Phase Transition Mechanism of VO2Films,” Journal of Physical Chemistry C, vol. 124, no. 31, pp. 17282–17289, Aug. 2020, doi: 10.1021/ACS.JPCC.0C03038/ASSET/IMAGES/LARGE/JP0C03038_0006.JPEG.

[36] R. Zhang et al., “Understanding of metal-insulator transition in VO 2 based on experimental and theoretical investigations of magnetic features,” vol. 8, p. 17093, 2018, doi: 10.1038/s41598-018-35490-5.

[37] C. Y. Kim, T. Slusar, J. Cho, and H. T. Kim, “Mott Switching and Structural Transition in the Metal Phase of VO2Nanodomain,” ACS Appl Electron Mater, vol. 3, no. 2, pp. 605–610, Feb. 2021, doi: 10.1021/ACSAELM.0C00983/SUPPL_FILE/EL0C00983_LIVESLIDES.MP4.

[38] C. Zhang, O. Gunes, S. J. Wen, Q. Yang, and S. Kasap, “Effect of Substrate Temperature on the Structural, Optical and Electrical Properties of DC Magnetron Sputtered VO2 Thin Films,” Materials 2022, Vol. 15, Page 7849, vol. 15, no. 21, p. 7849, Nov. 2022, doi: 10.3390/MA15217849.

[39] C. Zhang et al., “The Effect of Substrate Biasing during DC Magnetron Sputtering on the Quality of VO2 Thin Films and Their Insulator–Metal Transition Behavior,” Materials 2019, Vol. 12, Page 2160, vol. 12, no. 13, p. 2160, Jul. 2019, doi: 10.3390/MA12132160.

[40] C. Zhang et al., “Near-zero IR transmission of VO2 thin films deposited on Si substrate,” Appl Surf Sci, vol. 440, pp. 415–420, May 2018, doi: 10.1016/J.APSUSC.2018.01.176.

[41] C. Zhang et al., “Size, composition and alignment of VO2 microrod crystals by the reduction of V2O5 thin films, and their optical properties through insulator-metal transitions,” J Alloys Compd, vol. 827, p. 154150, Jun. 2020, doi: 10.1016/J.JALLCOM.2020.154150.

[42] C. Zhang et al., “Structural mapping of single-crystal VO2 microrods through metal-to-insulator phase transition,” J Mater Sci, vol. 56, no. 1, pp. 260–268, Jan. 2021, doi: 10.1007/S10853-020-05297-9/TABLES/2.

[43] P. P. Fedorov and E. G. Yarotskaya, “Zirconium dioxide. Review,” Condensed Matter and Interphases, vol. 23, no. 2, pp. 169–187, Jun. 2021, doi: 10.17308/KCMF.2021.23/3427.

[44] “The Nernst lamp in America,” Nature, vol. 64, no. 1669, pp. 632–633, 1901, doi: 10.1038/064632B0.

[45] A. Hojabri, “Structural and optical characterization of ZrO2 thin films grown on silicon and quartz substrates,” Journal of Theoretical and Applied Physics, vol. 10, no. 3, pp. 219–224, Sep. 2016, doi: 10.1007/S40094-016-0218-8/FIGURES/8.

[46] N. Ali, M. Bashir, S. Batool, S. Riaz, and S. Naseem, “Structural and Optical Properties of Zirconia Thin Films,” Mater Today Proc, vol. 2, no. 10, pp. 5771–5776, Jan. 2015, doi: 10.1016/J.MATPR.2015.11.126.

[47] C. Geng et al., “Influence of the thickness of ZrO2 buffer layer on the electrical and optical properties of VO2 films,” Infrared Phys Technol, vol. 102, p. 103016, Nov. 2019, doi: 10.1016/J.INFRARED.2019.103016.

[48] X. Gan, Z. Wang, B. Tian, Y. Xu, L. Li, and R. Xu, “Preparation of CeO2/TiO2 bilayer nanoparticle coating on ZrO2 fibers for thermal radiation shielding applications,” Mater Today Commun, vol. 37, p. 107480, Dec. 2023, doi: 10.1016/J.MTCOMM.2023.107480.

[49] Y. A. Abdelghany, M. M. Kassab, M. M. Radwan, and M. A. Abdel-Latif, “Borotellurite glass system doped with ZrO2, potential use for radiation shielding,” Progress in Nuclear Energy, vol. 149, p. 104256, Jul. 2022, doi: 10.1016/J.PNUCENE.2022.104256.

[50] X. Gan et al., “Preparation of a CeO2-nanoparticle thermal radiation shield coating on ZrO2 fibers via a hydrothermal method,” Ceram Int, vol. 43, no. 16, pp. 14183–14191, Nov. 2017, doi: 10.1016/J.CERAMINT.2017.07.161.

[51] K. Geng, Y. Xie, L. Yan, and B. Yan, “Fe-Si/ZrO2 composites with core-shell structure and excellent magnetic properties prepared by mechanical milling and spark plasma sintering,” J Alloys Compd, vol. 718, pp. 53–62, Sep. 2017, doi: 10.1016/J.JALLCOM.2017.05.114.

[52] J. D. Morrow, M. I. Tejedor-Anderson, M. A. Anderson, L. A. M. Ruotolo, F. E. Pfefferkorn, and M. Asme, “Synthesis and Characterization of ZrO2 Coatings on Micro End Mills With Sol–Gel Processing,” J Micro Nanomanuf, vol. 2, no. 4, Dec. 2014, doi: 10.1115/1.4028124.

[53] T. Norfauzi, A. B. Hadzley, U. A. A. Azlan, A. A. Afuza, M. M. Faiz, and M. F. Naim, “Fabrication and machining performance of ceramic cutting tool based on the Al2O3-ZrO2-Cr2O3 compositions,” Journal of Materials Research and Technology, vol. 8, no. 6, pp. 5114–5123, Nov. 2019, doi: 10.1016/J.JMRT.2019.08.034.

[54] L. A. Dobrzański and J. Mikuła, “The structure and functional properties of PVD and CVD coated Al2O3 + ZrO2 oxide tool ceramics,” J Mater Process Technol, vol. 167, no. 2–3, pp. 438–446, Aug. 2005, doi: 10.1016/J.JMATPROTEC.2005.05.034.

[55] E. A. Abdel Wahab, K. S. Shaaban, R. Elsaman, and E. S. Yousef, “Radiation shielding and physical properties of lead borate glass-doped ZrO2 nanoparticles,” Appl Phys A Mater Sci Process, vol. 125, no. 12, pp. 1–15, Dec. 2019, doi: 10.1007/S00339-019-3166-8/FIGURES/20.

[56] M. M. Mikhailov and A. S. Verevkin, “Optical properties and radiation stability of thermal control coatings based on doped zirconium dioxide powders,” J Mater Res, vol. 19, no. 2, pp. 535–541, 2004, doi: 10.1557/JMR.2004.19.2.535.

[57] J. Wu et al., “Facile Synthesis of Island-like ZrO2-VO2 Composite Films with Enhanced Thermochromic Performance for Smart Windows,” Materials, vol. 16, no. 1, Jan. 2023, doi: 10.3390/MA16010273.

[58] H. Zong et al., “ZrO2/VO2/ZrO2 sandwich structure with improved optical properties and weatherability for smart window application,” Appl Phys A Mater Sci Process, vol. 127, no. 6, pp. 1–11, Jun. 2021, doi: 10.1007/S00339-021-04623-5/FIGURES/11.

[59] D. Panda and T. Y. Tseng, “Growth, dielectric properties, and memory device applications of ZrO2 thin films,” Thin Solid Films, vol. 531, pp. 1–20, Mar. 2013, doi: 10.1016/J.TSF.2013.01.004.

[60] H. Chen, L. Tang, H. Luo, X. Yuan, and D. Zhang, “Modulation of ferroelectricity in atomic layer deposited HfO2/ZrO2 multilayer films,” Mater Lett, vol. 313, p. 131732, Apr. 2022, doi: 10.1016/J.MATLET.2022.131732.

[61] H. Zong et al., “Tuning the electrical and optical properties of ZrxOy/VO2 thin films by controlling the stoichiometry of ZrxOy buffer layer,” Appl Surf Sci, vol. 487, pp. 138–145, Sep. 2019, doi: 10.1016/J.APSUSC.2019.04.115.

[62] W. Ye and K. Fang, “Comparative study on structure and properties of ZnO thin films prepared by RF magnetron sputtering using pure metallic Zn target and ZnO ceramic target,” Surface Engineering, vol. 36, no. 1, pp. 49–54, Jan. 2020, doi: 10.1080/02670844.2018.1555214.

[63] W. Wu et al., “Design of Antireflection and Enhanced Thermochromic Properties of TiO2/VO2 Thin Films,” Adv Mater Interfaces, vol. 10, no. 15, p. 2202506, May 2023, doi: 10.1002/ADMI.202202506.

[64] C. Zhang et al., “Characterization of vanadium oxide thin films with different stoichiometry using Raman spectroscopy,” Thin Solid Films, vol. 620, pp. 64–69, Dec. 2016, doi: 10.1016/J.TSF.2016.07.082.

[65] S. Lafane, S. Malek, J. Nel, and S. Abdelli-Messaci, “Room temperature and high-pressure-pulsed laser deposition of nanocrystalline VO2 thin films on glass substrate: plasma and film analyses,” Appl Phys A Mater Sci Process, vol. 127, no. 1, pp. 1–12, Jan. 2021, doi: 10.1007/S00339-020-04174-1/FIGURES/12.

[66] D. Vernardou, M. E. Pemble, and D. W. Sheel, “The Growth of Thermochromic VO2 Films on Glass by Atmospheric-Pressure CVD: A Comparative Study of Precursors, CVD Methodology, and Substrates,” Chemical Vapor Deposition, vol. 12, no. 5, pp. 263–274, May 2006, doi: 10.1002/CVDE.200506419.

[67] D. Li, Y. Shan, F. Huang, and S. Ding, “Sol–gel preparation and characterization of SiO2 coated VO2 films with enhanced transmittance and high thermochromic performance,” Appl Surf Sci, vol. 317, pp. 160–166, Oct. 2014, doi: 10.1016/J.APSUSC.2014.08.042.

[68] I. Bilous, V. Deshko, and I. Sukhodub, “Parametric analysis of external and internal factors influence on building energy performance using non-linear multivariate regression models,” Journal of Building Engineering, vol. 20, pp. 327–336, Nov. 2018, doi: 10.1016/J.JOBE.2018.07.021.

[69] M. Santamouris, “Cooling the buildings – past, present and future,” Energy Build, vol. 128, pp. 617–638, Sep. 2016, doi: 10.1016/J.ENBUILD.2016.07.034.

[70] A. K. Shukla, K. Sudhakar, and P. Baredar, “Exergetic assessment of BIPV module using parametric and photonic energy methods: A review,” Energy Build, vol. 119, pp. 62–73, May 2016, doi: 10.1016/J.ENBUILD.2016.03.022.

[71] U. Energy Information Administration, “Annual Energy Outlook 2023: Narrative,” 2023.

[72] S. Domjan, C. Arkar, Ž. Begelj, and S. Medved, “Evolution of all-glass nearly Zero Energy Buildings with respect to the local climate and free-cooling techniques,” Build Environ, vol. 160, p. 106183, Aug. 2019, doi: 10.1016/J.BUILDENV.2019.106183.

[73] H. J. An, J. H. Yoon, Y. S. An, and E. Heo, “Heating and Cooling Performance of Office Buildings with a-Si BIPV Windows Considering Operating Conditions in Temperate Climates: The Case of Korea,” Sustainability 2018, Vol. 10, Page 4856, vol. 10, no. 12, p. 4856, Dec. 2018, doi: 10.3390/SU10124856.

[74] C. Zhang, C. Xi, Z. Feng, J. Wang, and S. J. Cao, “Passive design for green buildings by using green glass space and earth air tunnel,” Energy Build, vol. 273, p. 112367, Oct. 2022, doi: 10.1016/J.ENBUILD.2022.112367.

[75] A. Thongtha and P. Boontham, “Experimental Investigation of Natural Lighting Systems Using Cylindrical Glass for Energy Saving in Buildings,” Energies 2020, Vol. 13, Page 2528, vol. 13, no. 10, p. 2528, May 2020, doi: 10.3390/EN13102528.

[76] C. Ji et al., “Al-doped VO2 films as smart window coatings: reduced phase transition temperature and improved thermochromic performance,” Solar Energy Materials and Solar Cells, vol. 176, pp. 174–180, Mar. 2018, doi: 10.1016/J.SOLMAT.2017.11.026.

[77] Z. Xiang et al., “Optimized thermochromic properties for smart window application of VO2 films by wet-etching process,” Opt Mater (Amst), vol. 128, p. 112359, Jun. 2022, doi: 10.1016/J.OPTMAT.2022.112359.

[78] Y. Gao et al., “Nanoceramic VO 2 thermochromic smart glass: A review on progress in solution processing,” Nano Energy, vol. 1, pp. 221–246, 2012, doi: 10.1016/j.nanoen.2011.12.002.

[79] Y. Cui et al., “Thermochromic VO 2 for Energy-Efficient Smart Windows,” Joule, vol. 2, pp. 1707–1746, 2018, doi: 10.1016/j.joule.2018.06.018.

[80] M. BenKahoul et al., “Multilayer tuneable emittance coatings, with higher emittance for improved smart thermal control in space applications,” in 40th International Conference on Environmental Systems, ICES 2010, 2010. doi: 10.2514/6.2010-6266.

[81] B. Xie et al., “VO2 particle-based intelligent metasurface with perfect infrared emission for the spacecraft thermal control,” Applied Optics, Vol. 61, Issue 35, pp. 10538-10547, vol. 61, no. 35, pp. 10538–10547, Dec. 2022, doi: 10.1364/AO.475672.

[82] H. Wyers, “SOME TOXIC EFFECTS OF VANADIUM PENTOXIDE”.

[83] J. M. Wörle-Knirsch, K. Kern, C. Schleh, C. Adelhelm, C. Feldmann, and H. F. Krug, “Nanoparticulate vanadium oxide potentiated vanadium toxicity in human lung cells,” Environ Sci Technol, vol. 41, no. 1, pp. 331–336, Jan. 2007, doi: 10.1021/ES061140X/SUPPL_FILE/ES061140XSI20060917_075706.PDF.

[84] M. Rojas-Lemus et al., “Toxic Effects of Inhaled Vanadium Attached to Particulate Matter: A Literature Review,” International Journal of Environmental Research and Public Health 2021, Vol. 18, Page 8457, vol. 18, no. 16, p. 8457, Aug. 2021, doi: 10.3390/IJERPH18168457.

[85] M. A. Gadalla, “Prediction of temperature variation in a rotating spacecraft in space environment,” Appl Therm Eng, vol. 25, no. 14–15, pp. 2379–2397, Oct. 2005, doi: 10.1016/J.APPLTHERMALENG.2004.12.018.

[86] B. F. James, O. W. Coordinator, M. B. Norton, and M. Alexander, “NASA Reference Publication 1350 The Natural Space Environment: Effects on Spacecraft,” 1994.

[87] Vest, “THE EFFECTS OF THE SPACE ENVIROMENT ON SPACECRAFT SURFACES”.

[88] N. O. Borshchev, A. E. Sorokin, and A. E. Belyavskii, “External Heating of Spacecraft,” Russian Engineering Research, vol. 40, no. 2, pp. 168–170, Feb. 2020, doi: 10.3103/S1068798X20020057/FIGURES/2.

[89] H. Kim et al., “VO2-based switchable radiator for spacecraft thermal control,” Scientific Reports 2019 9:1, vol. 9, no. 1, pp. 1–8, Aug. 2019, doi: 10.1038/s41598-019-47572-z.

[90] S. S. Technology, “2022 State of the Art Small Spacecraft Technology Report,” 2023, Accessed: Sep. 12, 2023. [Online]. Available: http://www.sti.nasa.gov

[91] T. D. Swanson and G. C. Birur, “NASA thermal control technologies for robotic spacecraft,” Appl Therm Eng, vol. 23, no. 9, pp. 1055–1065, Jun. 2003, doi: 10.1016/S1359-4311(03)00036-X.

[92] A. S. L. F. P. I. D. P. D. Theodore L. Bergman, Fundamentals of Heat and Mass Transfer, vol. 7. John Wiley & Sons, Inc. (2011), 2018.

[93] Y. Shimakawa et al., “A variable-emittance radiator based on a metal-insulator transition of thin films,” Appl. Phys. Lett, vol. 80, pp. 4864–4866, 2002, doi: 10.1063/1.1489079.

[94] K. Sun et al., “VO2 Thermochromic Metamaterial-Based Smart Optical Solar Reflector,” ACS Photonics, vol. 5, no. 6, pp. 2280–2286, Jun. 2018, doi: 10.1021/ACSPHOTONICS.8B00119/SUPPL_FILE/PH8B00119_SI_001.PDF.

[95] S. Kabir et al., “Phase change vanadium dioxide light sensors,” Appl Mater Today, vol. 21, p. 100833, Dec. 2020, doi: 10.1016/J.APMT.2020.100833.

[96] H. T. Zhang et al., “Imprinting of Local Metallic States into VO2 with Ultraviolet Light,” Adv Funct Mater, vol. 26, no. 36, pp. 6612–6618, Sep. 2016, doi: 10.1002/ADFM.201601890.

[97] A. Cavalleri et al., “Femtosecond Structural Dynamics in VO 2 during an Ultrafast Solid-Solid Phase Transition,” 2001, doi: 10.1103/PhysRevLett.87.237401.

[98] G. Li et al., “Flexible VO2 Films for In-Sensor Computing with Ultraviolet Light,” Adv Funct Mater, vol. 32, no. 29, p. 2203074, Jul. 2022, doi: 10.1002/ADFM.202203074.

[99] G. Li et al., “Photo-induced non-volatile VO2 phase transition for neuromorphic ultraviolet sensors,” Nature Communications 2022 13:1, vol. 13, no. 1, pp. 1–9, Apr. 2022, doi: 10.1038/s41467-022-29456-5.

[100] A. Simo, B. Mwakikunga, B. T. Sone, B. Julies, R. Madjoe, and M. Maaza, “VO2 nanostructures based chemiresistors for low power energy consumption hydrogen sensing,” Int J Hydrogen Energy, vol. 39, no. 15, pp. 8147–8157, May 2014, doi: 10.1016/J.IJHYDENE.2014.03.037.

[101] J. Min Baik et al., “Pd-Sensitized Single Vanadium Oxide Nanowires: Highly Responsive Hydrogen Sensing Based on the Metal-Insulator Transition,” Nano Lett, vol. 9, no. 12, pp. 3980–3984, 2009, doi: 10.1021/nl902020t.

[102] E. Strelcov, Y. Lilach, and A. Kolmakov, “Gas sensor based on metal-insulator transition in VO 2 nanowire thermistor,” Nano Lett, vol. 9, no. 6, pp. 2322–2326, Jun. 2009, doi: 10.1021/NL900676N/SUPPL_FILE/NL900676N_SI_001.PDF.

[103] B. Cabrera, R. M. Clarke, P. Colling, A. J. Miller, S. Nam, and R. W. Romani, “Detection of single infrared, optical, and ultraviolet photons using superconducting transition edge sensors,” Appl Phys Lett, vol. 73, no. 6, pp. 735–737, Aug. 1998, doi: 10.1063/1.121984.

[104] L. Hu et al., “Porous W-doped VO2 films with simultaneously enhanced visible transparency and thermochromic properties,” J Solgel Sci Technol, vol. 77, no. 1, pp. 85–93, Jan. 2016, doi: 10.1007/S10971-015-3832-Z/FIGURES/7.

[105] A. V. Ivanov et al., “Fabrication of Epitaxial W-Doped VO2Nanostructured Films for Terahertz Modulation Using the Solvothermal Process,” ACS Appl Nano Mater, vol. 4, no. 10, pp. 10592–10600, Oct. 2021, doi: 10.1021/ACSANM.1C02081/ASSET/IMAGES/LARGE/AN1C02081_0010.JPEG.

[106] X. Chen et al., “Tuning the Doping Ratio and Phase Transition Temperature of VO2 Thin Film by Dual-Target Co-Sputtering,” Nanomaterials 2019, Vol. 9, Page 834, vol. 9, no. 6, p. 834, Jun. 2019, doi: 10.3390/NANO9060834.

[107] C. L. Gomez-Heredia et al., “Measurement of the hysteretic thermal properties of W-doped and undoped nanocrystalline powders of VO2,” Scientific Reports 2019 9:1, vol. 9, no. 1, pp. 1–14, Oct. 2019, doi: 10.1038/s41598-019-51162-4.

[108] M. K. Dietrich, B. G. Kramm, M. Becker, B. K. Meyer, A. Polity, and P. J. Klar, “Influence of doping with alkaline earth metals on the optical properties of thermochromic VO2,” J Appl Phys, vol. 117, no. 18, p. 185301, May 2015, doi: 10.1063/1.4919433/966202.

[109] L. Dai et al., “F-doped VO2 nanoparticles for thermochromic energy-saving foils with modified color and enhanced solar-heat shielding ability,” Physical Chemistry Chemical Physics, vol. 15, no. 28, pp. 11723–11729, Jul. 2013, doi: 10.1039/C3CP51359A.

[110] C. Piccirillo, R. Binions, and I. P. Parkin, “Nb-Doped VO2 Thin Films Prepared by Aerosol-Assisted Chemical Vapour Deposition,” Eur J Inorg Chem, vol. 2007, no. 25, pp. 4050–4055, Sep. 2007, doi: 10.1002/EJIC.200700284.

[111] N. Shen et al., “The synthesis and performance of Zr-doped and W-Zr-codoped VO 2 nanoparticles and derived flexible foils,” 2014, doi: 10.1039/c4ta02880e.

[112] C. Lu, W. Liang, M. Gao, S. N. Luo, and Y. Lin, “Terahertz Transmittance of Cobalt-Doped VO2 Thin Film: Investigated by Terahertz Spectroscopy and Effective Medium Theory,” IEEE Trans Terahertz Sci Technol, vol. 9, no. 2, pp. 177–185, Mar. 2019, doi: 10.1109/TTHZ.2019.2894516.

[113] X. Zhou, D. Gu, Y. Li, Z. Sun, Y. Jiang, and Y. Long, “Abnormal dependence of microstructures and electrical properties of Y-doped VO2 thin films on deposition temperature,” Ceram Int, vol. 46, no. 11, pp. 18315–18321, Aug. 2020, doi: 10.1016/J.CERAMINT.2020.05.053.

[114] D. Gu, X. Zhou, Z. Sun, and Y. Jiang, “Influence of Gadolinium-doping on the microstructures and phase transition characteristics of VO2 thin films,” J Alloys Compd, vol. 705, pp. 64–69, May 2017, doi: 10.1016/J.JALLCOM.2017.02.138.

[115] S. Wang et al., “Al-Doping-Induced VO2 (B) Phase in VO2 (M) Toward Smart Optical Thin Films with Modulated ΔTvis and ΔTc,” Adv Eng Mater, vol. 21, no. 12, p. 1900947, Dec. 2019, doi: 10.1002/ADEM.201900947.

[116] A. Muller et al., “Radio-Frequency Characteristics of Ge-Doped Vanadium Dioxide Thin Films with Increased Transition Temperature,” ACS Appl Electron Mater, vol. 2, no. 5, pp. 1263–1272, May 2020, doi: 10.1021/ACSAELM.0C00078/ASSET/IMAGES/LARGE/EL0C00078_0003.JPEG.

[117] N. Wang, S. Liu, X. T. Zeng, S. Magdassi, and Y. Long, “Mg/W-codoped vanadium dioxide thin films with enhanced visible transmittance and low phase transition temperature,” J Mater Chem C Mater, vol. 3, no. 26, pp. 6771–6777, Jun. 2015, doi: 10.1039/C5TC01062D.

[118] Plasmonique Inc., “Magnetron Sputter Deposition System Model SPT320 Operation Manual,” 2015. [Online]. Available: www.plasmionique.com

[119] Masoud Mohammad Taheri, “Synthesis and Characterization of Hard Cr 2 O 3 and Superhard Cr-Zr-O PVD Coatings,” Dissertation, University of Saskatchewan, Saskatoon, 2019.

[120] D. W. Shipp, F. Sinjab, and I. Notingher, “Raman spectroscopy: techniques and applications in the life sciences,” Advances in Optics and Photonics, Vol. 9, Issue 2, pp. 315-428, vol. 9, no. 2, pp. 315–428, Jun. 2017, doi: 10.1364/AOP.9.000315.

[121] C. Zhang et al., “Synthesis, structure and optical properties of high-quality VO2 thin films grown on silicon, quartz and sapphire substrates by high temperature magnetron sputtering: Properties through the transition temperature,” J Alloys Compd, vol. 848, p. 156323, Dec. 2020, doi: 10.1016/J.JALLCOM.2020.156323.

[122] R. Swanepoel, “Determination of the thickness and optical constants of amorphous silicon,” J Phys E, vol. 16, no. 12, p. 1214, Dec. 1983, doi: 10.1088/0022-3735/16/12/023.

[123] T. M. Arantes et al., “Stable colloidal suspensions of nanostructured zirconium oxide synthesized by hydrothermal process,” Journal of Nanoparticle Research, vol. 12, no. 8, pp. 3105–3110, Oct. 2010, doi: 10.1007/S11051-010-9906-5/FIGURES/5.

[124] K. Pan, W. Wang, E. Shin, K. Freeman, and G. Subramanyam, “Vanadium Oxide Thin-Film Variable Resistor-Based RF Switches,” IEEE Trans Electron Devices, vol. 62, no. 9, pp. 2959–2965, Sep. 2015, doi: 10.1109/TED.2015.2451993.

[125] L. Bi et al., “Study of the phase evolution, metal-insulator transition, and optical properties of vanadium oxide thin films,” Optical Materials Express, Vol. 6, Issue 11, pp. 3609-3621, vol. 6, no. 11, pp. 3609–3621, Nov. 2016, doi: 10.1364/OME.6.003609.

[126] B. Van Bilzen et al., “Production of VO2 thin films through post-deposition annealing of V2O3 and VOx films,” Thin Solid Films, vol. 591, pp. 143–148, Sep. 2015, doi: 10.1016/J.TSF.2015.08.036.

[127] N. K. Jayswal, I. Subedi, A. Shan, and N. J. Podraza, “Tracking optical properties of VOx films to optimize polycrystalline VO2 fabrication,” Thin Solid Films, vol. 798, p. 140367, Jun. 2024, doi: 10.1016/J.TSF.2024.140367.

[128] C. Geng et al., “Influence of the thickness of ZrO2 buffer layer on the electrical and optical properties of VO2 films,” Infrared Phys Technol, vol. 102, p. 103016, Nov. 2019, doi: 10.1016/J.INFRARED.2019.103016.

[129] A. S. Hassanien, H. R. Alamri, and I. M. El Radaf, “Impact of film thickness on optical properties and optoelectrical parameters of novel CuGaGeSe4 thin films synthesized by electron beam deposition,” Opt Quantum Electron, vol. 52, no. 7, pp. 1–18, Jul. 2020, doi: 10.1007/S11082-020-02448-9/FIGURES/12.

[130] R. Nasrin, H. Kabir, H. Akter, and A. H. Bhuiyan, “Effect of film thickness on topographic, microstructural, optical and dielectric behaviour of PPMBA thin films,” Results Phys, vol. 19, p. 103357, Dec. 2020, doi: 10.1016/J.RINP.2020.103357.

[131] Y. Yang et al., “Thickness effects on the epitaxial strain states and phase transformations in (001)-VO2/TiO2 thin films,” J Appl Phys, vol. 125, no. 8, p. 82508, Feb. 2019, doi: 10.1063/1.5049551/133396.

[132] C. Zhang, O. Gunes, S. J. Wen, Q. Yang, and S. Kasap, “Effect of Substrate Temperature on the Structural, Optical and Electrical Properties of DC Magnetron Sputtered VO2 Thin Films,” Materials 2022, Vol. 15, Page 7849, vol. 15, no. 21, p. 7849, Nov. 2022, doi: 10.3390/MA15217849.

[133] C. Zhang et al., “Near-zero IR transmission of VO2 thin films deposited on Si substrate,” Appl Surf Sci, vol. 440, pp. 415–420, May 2018, doi: 10.1016/J.APSUSC.2018.01.176.

[134] C. Geng et al., “Influence of the thickness of ZrO2 buffer layer on the electrical and optical properties of VO2 films,” Infrared Phys Technol, vol. 102, p. 103016, Nov. 2019, doi: 10.1016/J.INFRARED.2019.103016.

[135] C. Zhang, O. Gunes, S. J. Wen, Q. Yang, and S. Kasap, “Effect of Substrate Temperature on the Structural, Optical and Electrical Properties of DC Magnetron Sputtered VO2 Thin Films,” Materials 2022, Vol. 15, Page 7849, vol. 15, no. 21, p. 7849, Nov. 2022, doi: 10.3390/MA15217849.

[136] G. Xu, P. Jin, M. Tazawa, and K. Yoshimura, “Optimization of antireflection coating for VO2-based energy efficient window,” Solar Energy Materials and Solar Cells, vol. 83, no. 1, pp. 29–37, Jun. 2004, doi: 10.1016/J.SOLMAT.2004.02.014.

[137] R. W. G. Hunt, “Appendix 7: Spectral Luminous Efficiency Functions,” The Reproduction of Colour, pp. 678–679, Sep. 2004, doi: 10.1002/0470024275.APP7.

[138] “Reference Air Mass 1.5 Spectra | Grid Modernization | NREL.” Accessed: Mar. 03, 2024. [Online]. Available: https://www.nrel.gov/grid/solar-resource/spectra-am1.5.html